U.S. Department
of Transportation

Federal Railroad Administration

Deformation Behavior of Welded Steel Sandwich Panels under Quasi-Static Loading

Office of Railroad Policy
and Development
Washington, DC 20590

DOT/FRA/ORD-11/06

Final Report
March 2011

NOTICE

This document is disseminated under the sponsorship of the Department of Transportation in the interest of information exchange. The United States Government assumes no liability for its content or use thereof.

NOTICE

The United States Government does not endorse products or manufacturers. Trade or manufacturers' names appear herein solely because they are considered essential to the object of this report.

REPORT DOCUMENTATION PAGE

Form Approved OMB No. 0704-0188

1. AGENCY USE ONLY (Leave blank)	2. REPORT DATE March 2011	3. REPORT TYPE AND DATES COVERED Technical Report

4. TITLE AND SUBTITLE
Deformation Behavior of Welded Steel Sandwich Panels Under Quasi-Static Loading

5. FUNDING NUMBERS
RR-28/HG-034
RR-28A1/HG-269
RR-93/HG-284

6. AUTHOR(S)
D. Y. Jeong, M. E. Carolan, A. B. Perlman, and Y. H. Tang

7. PERFORMING ORGANIZATION NAME(S) AND ADDRESS(ES)
U.S. Department of Transportation
Volpe National Transportation Systems Center
Research and Innovative Technology Administration
55 Broadway
Cambridge, MA 02142-1093

8. PERFORMING ORGANIZATION REPORT NUMBER
DOT-VNTSC-FRA-10-08

9. SPONSORING/MONITORING AGENCY NAME(S) AND ADDRESS(ES)
Federal Railroad Administration
Office of Railroad Policy and Development
1200 New Jersey Avenue, SE
Washington, DC 20590

10. SPONSORING/MONITORING AGENCY REPORT NUMBER
DOT/FRA/ORD-11/06

11. SUPPLEMENTARY NOTES
Program Manager: Francisco González III

12a. DISTRIBUTION/AVAILABILITY STATEMENT
This document is available to the public through the FRA Web site at http://www.fra.dot.gov.

12b. DISTRIBUTION CODE

13. ABSTRACT (Maximum 200 words)

This report describes engineering studies that were conducted to examine the deformation behavior of flat, welded steel sandwich panels under two quasi-static loading conditions: (1) uniaxial compression; and (2) bending with an indenter. Testing and analysis are conducted to study the force-displacement response of sandwich structures with different core geometries: (1) pipe or tubular cores with outer diameters equal to 2, 3, and 5 in; (2) a 2-inch square diamond core; and (3) a double corrugated core called an X-core with a 5-inch core height. Deformation and local collapse modes of sandwich panels under these loading conditions are also studied. Moreover, the work described in this report represents basic research to investigate the concept of applying welded steel sandwich structures as a means to offer protection to railroad tank cars—especially those carrying hazardous materials—in the event of an accident.

14. SUBJECT TERMS
Bending, compression, core geometry, face sheet, sandwich structure

15. NUMBER OF PAGES
71

16. PRICE CODE

17. SECURITY CLASSIFICATION OF REPORT	18. SECURITY CLASSIFICATION OF THIS PAGE	19. SECURITY CLASSIFICATION OF ABSTRACT	20. LIMITATION OF ABSTRACT
Unclassified	Unclassified	Unclassified	

NSN 7540-01-280-5500

Standard Form 298 (Rev. 2-89)
Prescribed by ANSI Std. 239-18
298-102

METRIC/ENGLISH CONVERSION FACTORS

ENGLISH TO METRIC

LENGTH (APPROXIMATE)

1 inch (in)	=	2.5 centimeters (cm)
1 foot (ft)	=	30 centimeters (cm)
1 yard (yd)	=	0.9 meter (m)
1 mile (mi)	=	1.6 kilometers (km)

AREA (APPROXIMATE)

1 square inch (sq in, in^2)	=	6.5 square centimeters (cm^2)
1 square foot (sq ft, ft^2)	=	0.09 square meter (m^2)
1 square yard (sq yd, yd^2)	=	0.8 square meter (m^2)
1 square mile (sq mi, mi^2)	=	2.6 square kilometers (km^2)
1 acre = 0.4 hectare (he)	=	4,000 square meters (m^2)

MASS - WEIGHT (APPROXIMATE)

1 ounce (oz)	=	28 grams (gm)
1 pound (lb)	=	0.45 kilogram (kg)
1 short ton = 2,000 pounds (lb)	=	0.9 tonne (t)

VOLUME (APPROXIMATE)

1 teaspoon (tsp)	=	5 milliliters (ml)
1 tablespoon (tbsp)	=	15 milliliters (ml)
1 fluid ounce (fl oz)	=	30 milliliters (ml)
1 cup (c)	=	0.24 liter (l)
1 pint (pt)	=	0.47 liter (l)
1 quart (qt)	=	0.96 liter (l)
1 gallon (gal)	=	3.8 liters (l)
1 cubic foot (cu ft, ft^3)	=	0.03 cubic meter (m^3)
1 cubic yard (cu yd, yd^3)	=	0.76 cubic meter (m^3)

TEMPERATURE (EXACT)

[(x-32)(5/9)] °F	=	y °C

METRIC TO ENGLISH

LENGTH (APPROXIMATE)

1 millimeter (mm)	=	0.04 inch (in)
1 centimeter (cm)	=	0.4 inch (in)
1 meter (m)	=	3.3 feet (ft)
1 meter (m)	=	1.1 yards (yd)
1 kilometer (km)	=	0.6 mile (mi)

AREA (APPROXIMATE)

1 square centimeter (cm^2)	=	0.16 square inch (sq in, in^2)
1 square meter (m^2)	=	1.2 square yards (sq yd, yd^2)
1 square kilometer (km^2)	=	0.4 square mile (sq mi, mi^2)
10,000 square meters (m^2)	=	1 hectare (ha) = 2.5 acres

MASS - WEIGHT (APPROXIMATE)

1 gram (gm)	=	0.036 ounce (oz)
1 kilogram (kg)	=	2.2 pounds (lb)
1 tonne (t)	=	1,000 kilograms (kg)
	=	1.1 short tons

VOLUME (APPROXIMATE)

1 milliliter (ml)	=	0.03 fluid ounce (fl oz)
1 liter (l)	=	2.1 pints (pt)
1 liter (l)	=	1.06 quarts (qt)
1 liter (l)	=	0.26 gallon (gal)
1 cubic meter (m^3)	=	36 cubic feet (cu ft, ft^3)
1 cubic meter (m^3)	=	1.3 cubic yards (cu yd, yd^3)

TEMPERATURE (EXACT)

[(9/5) y + 32] °C	=	x °F

QUICK INCH - CENTIMETER LENGTH CONVERSION

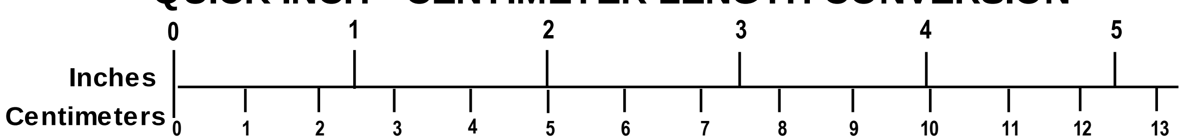

QUICK FAHRENHEIT - CELSIUS TEMPERATURE CONVERSION

°F	-40°	-22°	-4°	14°	32°	50°	68°	86°	104°	122°	140°	158°	176°	194°	212°
°C	-40°	-30°	-20°	-10°	0°	10°	20°	30°	40°	50°	60°	70°	80°	90°	100°

For more exact and or other conversion factors, see NIST Miscellaneous Publication 286, Units of Weights and Measures. Price $2.50 SD Catalog No. C13 10286

Updated 6/17/98

Preface

The Federal Railroad Administration (FRA), Office of Railroad Policy and Development, sponsored the work described in this report. Specifically, this work was conducted and managed by the Structures and Dynamics Division of the John A. Volpe National Transportation Systems Center (Volpe Center) through Project Plan Agreements and Inter-Agency Agreements with FRA. Moreover, this work is carried out through two Volpe Center projects: Tank Car Structural Integrity in FRA's Rail Equipment Safety Research Program and Improved Tank Car Design Development in FRA's Railroad Systems Safety Research Program. Mr. Kevin Kesler is the Chief of the Equipment and Operating Practices Research Division. Mr. Francisco González III is the project manager for research on railroad tank cars and hazardous materials.

Contents

Executive Summary **1**

1 Introduction **4**

2 Sandwich Panel Characteristics **7**

3 Behavior under Uniaxial Compression **15**

3.1 Quasi-Static Compression Tests 18
3.2 Comparisons with Analysis 21

4 Behavior under Bending with an Indenter **25**

4.1 Local Collapse Modes 27
4.2 Quasi-Static Bend Tests 31

5 Summary of Test and Analysis Results **35**

6 Discussion **37**

7 References **41**

Appendix A. Force-Crush Curves from Compression Tests **44**

Appendix B. Estimation of Core Strength by Limit Analysis **47**

Appendix C. Force-Displacement Curves from Bend Tests and Analyses **58**

Abbreviations and Symbols **63**

Illustrations

Figure 1. Percent of Damage by Location on Insulated Tank Cars in Mainline Accidents 5

Figure 2. Strength Properties of Sandwich Panel Materials 12

Figure 3. Ductility of Sandwich Panel Materials... 13

Figure 4. Schematic Force-Crush Response of Sandwich Panel with Idealized Elastic-Plastic Core Material to Uniaxial Compression.. 16

Figure 5. Generic Force-Crush Response of Pipe Core Sandwich Panel 16

Figure 6. Generic Force-Crush Response of Diamond Core Sandwich Panel 17

Figure 7. Generic Force-Crush Response of X-Core Sandwich Panel 18

Figure 8. Variation of Compressive Strength with Relative Density 20

Figure 9. Variation of Theoretical and Measured Strength of Pipe Cores with Relative Density 22

Figure 10. Variation of Theoretical and Measured Strength of Diamond Core with Relative Density 23

Figure 11. Measured and Calculated Force-Crush Curves for 5-Inch Pipe Core 23

Figure 12. Predicted and Observed Deformation of 5-Inch Pipe Core....................................... 24

Figure 13. Closeup View of Final Deformation Mode in 5-Inch Pipe Core............................... 24

Figure 14. Schematic of Bend Test Configuration 25

Figure 15. Schematic Force-Displacement Curve in Bend Test.. 26

Figure 16. Possible Local Collapse Modes in Bending 27

Figure 17. Collapse Mechanism Map for 3-Inch Pipe Core Panel in Bending............................ 28

Figure 18. Collapse Mechanism Map for Diamond Core Panel in Bending 29

Figure 19. Photograph of Face Sheet Fracture from Quasi-Static Bend Test.............................. 29

Figure 20. Bend Test with Bubble Wrap to Quantify Load Spreading 30

Figure 21. Collapse Loads in Bend Tests 33

Figure 22. Comparison of Compressive Strength for Different Cores 39

Tables

Table 1. Recent Railroad Hazmat Accidents 4
Table 2. Details of Pipe Core Panels 8
Table 3. Details of Diamond Core Panels 9
Table 4. Details of X-Core Panels 10
Table 5. Tensile Properties of Sandwich Panel Materials 11
Table 6. Tensile Property Specifications for TC-128B Steel 11
Table 7. Relative Densities for Different Cores 14
Table 8. Quasi-Static Compression Test Matrix 19
Table 9. Quasi-Static Bend Test Matrix 32

Executive Summary

This report describes basic research (i.e., testing and analysis) conducted to examine the deformation behavior of flat-welded steel sandwich panels under two types of quasi-static loading: (1) uniaxial compression and (2) bending through an indenter. The objectives of these tests were to (1) confirm the analytical and computational (i.e., finite element) modeling of sandwich structures, (2) examine the fabrication issues associated with such structures (e.g., material selection and welding processes), and (3) observe the deformation behavior and local collapse mechanisms under the two different types of loading. In addition, the uniaxial compression tests were performed to rank or screen different core geometries. Five core geometries were examined in the compression tests: pipe or tubular cores with outer diameters equal to 2, 3, and 5 inches; a 2-inch square diamond core; and a double-corrugated core called an X-core with a 5-inch core height.

Previous research conducted by the Federal Railroad Administration's (FRA) Office of Research and Development and the John A. Volpe National Transportation Systems Center (Volpe Center) included applying semi-empirical and computational (i.e., finite element analysis) methods to estimate the puncture resistance of conventional railroad tank cars under generalized head and shell impact scenarios. Subsequent work identified sandwich structures as a potential technology to improve the puncture resistance of the commodity-carrying tank under impact loading conditions.

Test articles for the compression and bend tests were manufactured by Cellular Materials International, Inc. (CMI), located in Charlottesville, VA. CMI was under contract with FRA through the Small Business Innovation Research Program. Test articles include the flat welded steel sandwich panels, plates to support the panels in the text fixture, and the indenter for the bend tests. Test panels were fabricated with materials that were readily available in the desired quantities at the time of construction.

Quasi-static tests were carried out using a 5-million-pound capacity universal testing machine by the Center for Advanced Technology for Large Structural Systems at Lehigh University's Fritz Engineering Laboratory in Bethlehem, PA. Uniaxial compression tests were conducted on 14 sandwich panels on May 7, 2009. Panel dimensions were approximately 24 inches in length and 6 inches in width. Deformation and crushing of the different cores were measured and observed as uniform pressure was applied onto the face sheets over an area of about 1 square foot (1 ft^2).

The compression tests showed excellent repeatability of structural (i.e., force-crush) response for panels with similar cores and welding. Compressive strength was estimated using plastic limit load analysis and shown to be in excellent agreement for the sandwich panels with pipe cores. Similar estimates for the diamond cores overpredict the measured strength. The 3-inch pipe core and the diamond core were selected as candidate cores for the next series of tests, because they possess attributes of moderate strength and moderate relative density. In addition, force-crush curves calculated from finite element analysis were in reasonable agreement with the measured curves for all cores.

Bend tests using a 12-inch by 12-inch indenter with 1-inch-radius rounded edges were conducted on 16 sandwich panels on December 9 and 10, 2009. The dimensions of the bend panels were approximately 48 in long by 18 in wide. The panels were simply supported over 4-inch-diameter rollers spanning 24 in between the centers of the rollers. The bend tests included three variables: (1) core type (diamond core and 3-inch pipe core); (2) core orientation relative to the supports (cores running either parallel or perpendicular to the rollers used to support the panels); and (3) face sheet type (solid plates on both sides, strips used as face sheets on both sides, and a combination of solid plates and strips). Force-displacement (i.e., head travel) curves were recorded during each test. Force levels were read off these curves, which were used to characterize the local collapse load of the sandwich panels in bending and to quantify the relative effects of the test variables. On the basis of this metric, the diamond core panels were shown to have slightly higher bending strength than the pipe core panels when solid face sheets were used. The difference in bending strength is almost negligible when strip face sheets were used. Bending strength of the panels was demonstrated to be strongly anisotropic. Panels with cores perpendicular to the supports had much higher bending strength than those with cores parallel to the supports. Panels with solid face sheets on both sides were shown to have higher bending strength than those with strips as face sheets.

Finite element analysis of the bend tests produced nearly identical shapes to the measured force-displacement curves. The computational modeling, however, overpredicts the force in the force-displacement curves compared with the test data in each case. The discrepancy is attributed to modeling perfect geometry, whereas imperfections likely exist in the actual test specimens.

Sandwich structures are now being used in applications such as impact-attenuation devices in the event of run-off-the-highway accidents and as protection for ship hulls against impulsive loading from blasts and explosions. The potential merits of using sandwich structures investigation for railroad applications have been identified in this research project. However, fundamental research is needed to evaluate the performance characteristics of sandwich structures under controlled loading conditions that are representative of the intended application.

The crushing and the bending characteristics of sandwich structures with the different cores tested under quasi-static loading can be incorporated into detailed finite element analyses that may eventually include fluid-structure interaction to account for the lading as well as material failure to estimate tank puncture. Moreover, computational models can be used to extrapolate performance of sandwich structures with features not considered in the present work. Preliminary results from simulations of tank shells protected by sandwich panels were discussed at a meeting about the Next Generation Tank Car project. The next logical step in continuing the basic research to investigate the proof-of-concept is to modify the loading condition from quasi-static to dynamic impact. Introducing dynamic loading will allow for examination of inertial effects on the deformation behavior of sandwich structures as protective panels.

Sandwich structure design aspects such as weight and space considerations are beyond the scope of the work described in this report. However, such limitations have been discussed in previous work. The present work focuses on the basic mechanisms of deformation and failure associated with idealized loading conditions. As the potential for sandwich structures to adequately protect railroad tank cars becomes realized, industry interest in this technology may take hold. At this point, a cost-benefit analysis can be conducted; additional studies will be warranted to further examine the practical design aspects of this novel technology in railroad transportation applications.

For the past two decades, the Office of Research and Development (FRA) has sponsored research performed by the Volpe Center in safety matters related to the transportation of hazardous materials by railroad tank cars. This research is used to support government and industry efforts in resolving problems related to metal fatigue, fracture, and welding in the current fleet; structural behavior under derailment and collision scenarios; and improving standards and procedures for future railcar designs. Moreover, the Volpe Center has performed and managed research on the structural integrity of railroad tank cars under various loading conditions, ranging from normal operations to rare and extreme circumstances such as accident loading.

1. Introduction

Accidents involving the release of hazmat from rail cars during transport can result in fatalities, injuries, and evacuations of nearby towns, as well as property and sometimes environmental damage. Table 1 lists some of the recent railroad hazmat accidents investigated by the National Transportation Safety Board (NTSB). Since the train derailment that occurred in Minot, ND, on January 18, 2002, the safety performance of railroad tank cars during accidents has come under great scrutiny. For example, NTSB made a series of safety recommendations to FRA after the NTSB's investigation of the Minot derailment [1]. Subsequently, the government and industry initiated research activities to develop strategies to maintain structural integrity and improve the crashworthiness of railroad tank cars carrying hazmat during accidents.

Table 1. Recent Railroad Hazmat Accidents

Location	*Date*	*Type of Accident*
Minot, ND	January 18, 2002	Derailment
Macdona, TX	June 28, 2004	Collision
Graniteville, SC	January 6, 2005	Collision
Anding, MS	July 10, 2005	Collision
Texarkana, AR	October 15, 2005	Collision
New Brighton, PA	October 20, 2006	Derailment
Shephardsville, KY	January 16, 2007	Derailment
Oneida, NY	March 12, 2007	Derailment
Rockford, IL	June 19, 2009	Derailment

In some of the accidents listed in Table 1, the release of hazmat occurred from an impacting object (e.g., broken coupler) penetrating and puncturing the end (also called the head) or the side (also called the shell) of the commodity-carrying tank. The table also shows that these accidents were classified as either a derailment or a collision. Although accidents are rare events, caution must be exercised in making statistical inferences from small sample-size data. However, comprehensive studies of available accident data, which include FRA's Railroad Accident/Incident Reporting System (RAIRS) [2], indicate that derailments and collisions account for more than 90 percent of all hazmat-related accidents [3]. In addition, accident data on damage to tank cars is maintained by the Railroad Tank Car Safety Research and Test Project, which is cosponsored by the Railway Supply Institute (RSI) and the Association of American Railroads (AAR). A recent report [4] provides information on the relative frequency of damage to various regions of the head and the shell, and the associated losses of lading from these regions, for various tank car configurations (i.e., cars with and without jackets). Figure 1 shows a graphical depiction of the aggregate findings for insulated tank cars involved in mainline accidents. The figure indicates that damage can occur anywhere on the commodity tank, although it is more likely to occur below the horizontal centerline and near the ends of the car.

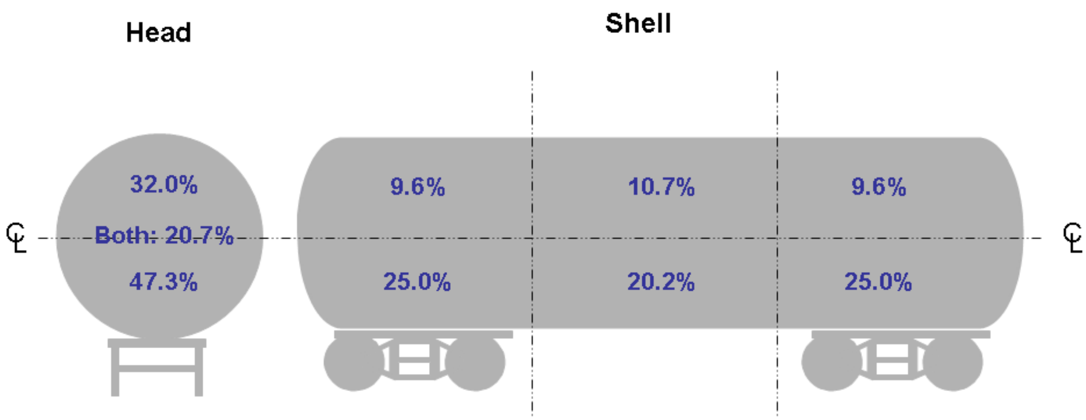

Figure 1. Percent of Damage by Location on Insulated Tank Cars in Mainline Accidents [4]

In 2004, the Volpe Center began conducting research to address the NTSB recommendations to FRA following the Minot, ND, derailment. This research included studies on derailment dynamics and the structural behavior of railroad tank cars during accidents [5]. Subsequent Volpe Center research identified sandwich structures technology as a potential technology to improve the crashworthiness of tank cars [6–8].

In 2006, the railroad industry began a research and development effort called the Next Generation Rail Tank Car (NGRTC) project to develop and implement tank car designs to improve safety performance. Dow Chemical Company, Union Pacific Railroad, and Union Tank Car were the industry sponsors of this project. In 2007, FRA and Transport Canada, two government regulatory agencies in North America, began collaborating with the NGRTC project through a Memoranda of Cooperation. Cooperative activities included full-scale shell impact testing of conventional tank cars designed to carry liquid chlorine. Separate activities included design development for improved crashworthiness. Government and industry collaboration in the NGRTC project dissolved in 2008.

One of the concepts considered during the government and industry research to improve crashworthiness of railroad tank cars proposed treating the commodity-carrying tank car as a protected entity. Moreover, welded steel sandwich structures were examined as a means to protect the commodity-carrying tank against penetrations and punctures from impacting objects in the event of a derailment or collision.

This report describes basic research, which entails testing and analysis conducted to examine the deformation behavior of flat-welded steel sandwich panels under quasi-static loading conditions. Specifically, two types of loads were applied: uniaxial compression and bending with an indenter. The objectives of these tests were to (1) confirm the analytical and computational (i.e., finite element) modeling of sandwich structures; (2) examine the fabrication issues associated with such structures (e.g., material selection and welding processes); and (3) observe the deformation behavior and local collapse mechanisms under the two different types of loading. In addition, uniaxial compression tests were performed to rank or screen different core geometries. The core geometries used in the compression tests were as follows: (1) pipe or tubular cores with outer diameters equal to 2, 3, and 5 in; (2) a 2-inch square diamond core; and (3) a double-corrugated core called an X-core with a 5-inch core height.

Test articles were manufactured by CMI, which is located in Charlottesville, VA, under contract with FRA through the Small Business Innovation Research Program. The compression and bend tests were conducted by the Center for Advanced Technology for Large Structural Systems (ATLSS) at Lehigh University's Fritz Engineering Laboratory in Bethlehem, PA. The analyses described in this report and the test designs were performed by the Volpe Center.

The organization of this report is as follows. Specific details of the sandwich panels used in the present work are described in Section 2. General descriptions and results on the behavior of sandwich panels subjected to uniaxial compression are given in Section 3. Force-crush measurements from individual quasi-static compression tests are provided in Appendix A. A detailed description of closed-form methods to interpret the compression test results is given in Appendix B. Generalizations on the behavior of sandwich panels subjected to bending with an indenter are given in Section 4. Force-displacement test data and comparisons with finite element results for the quasi-static bend tests are provided in Appendix C. Results from both quasi-static tests and the corresponding analyses are summarized in Section 5. Finally, suggestions for applying the results of the quasi-static tests and analyses to develop protective panels for railroad tank cars are discussed in Section 6.

2. Sandwich Panel Characteristics

Sandwich structures are generally composed of two face sheets that are separated by a core. In the traditional design of sandwich structures, the separation of the face sheets by the core increases the moment of inertia of the panel, which produces a higher bending stiffness-to-weight ratio than solid or monolithic plates. The face sheets carry almost all of the bending and in-plane loads while the core carries the shear load to prevent the face sheets from sliding past one another.

The work described in this report represents basic research that was used to investigate the concept of applying welded steel sandwich panels as a means to offer protection to the commodity-carrying tank against puncture in the event of a collision. In this concept, sandwich panels provide protection through two mechanisms: load blunting and energy absorption. Blunting means that the impact load is distributed over a larger area of the tank with respect to the indenter footprint, which effectively increases the energy needed to puncture the commodity-carrying tank. Protective panels also absorb collision energy, which decreases the effective impact speed felt by the commodity-carrying tank during impact. Moreover, the load-blunting and energy-absorbing capabilities of sandwich panels depend on the core shape or geometry.

The particular core geometries examined in this report are the following: (1) circular pipe or tubular cores with outer diameters equal to 2, 3, and 5 in; (2) a 2-inch square diamond core; and (3) a double corrugated core or X-core with a height of 5 in.

Table 2 shows a schematic of the unit cell for a pipe core. The table also lists the nominal dimensions of the pipe cores and the materials used to construct the cores and the face sheets. Similarly, Table 3 lists the specific details for the diamond core and Table 4 provides characteristics for the X-core. All of the sandwich panels in this study have face sheets with equal thickness.

In the present study, the forces produced from impact are decomposed into separate and idealized loads associated with crushing and bending of sandwich panels. By simplifying the application of loads, local collapse mechanisms can be observed and discriminated, which may help understand the failure mechanics of sandwich panels. The application of loads in a quasi-static manner allows for careful observation of the failure mechanisms while gathering data without the difficulties of dynamic (i.e., inertial) factors affecting instrumentation. Moreover, this basic research is intended to lay the foundation for improved puncture resistance for the commodity-carrying tank.

The core geometries described in this report have been examined previously for other applications. For example, impact-attenuation devices are used to decelerate an errant vehicle in the event of run-off-the-road highway accidents. Also known as crash cushions, the devices consist of clusters of mild steel cylinders or tubes that dissipate the impact energy [9, 10]. Pipe or tubular cores have also been considered in automobile applications as car bumpers and guardrails [11]. Research sponsored by the Office of Naval Research has been conducted on sandwich panels with diamond cores and X-cores to examine their application in protecting ship hulls against impulsive loads created by blasts and explosions [12–14].

Table 2. Details of Pipe Core Panels

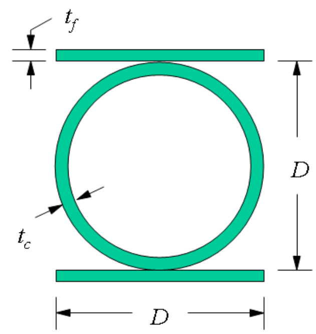

Core Characteristics	
Material	AISI 1010 steel
Pipe Outer Diameter, D	2, 3, and 5 in
Thickness, t_c	0.125 in
Face Sheet Characteristics	
Material	Domex (100XF) plate
Thickness, t_f	0.25 in for compression panels 0.118 in for bend panels

Table 3. Details of Diamond Core Panels

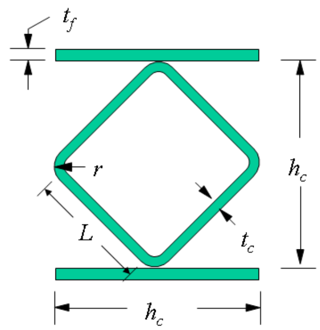

Core Characteristics	
Material	AISI 1010 steel
Height, h_c	2.62 in
Thickness, t_c	0.125 in
Leg Length, L	2 in
Corner Radius, r	0.25 in
Face Sheet Characteristics	
Material	Domex (100XF) plate
Thickness, t_f	0.25 in for compression panels 0.118 in for bend panels

Table 4. Details of X-Core Panels

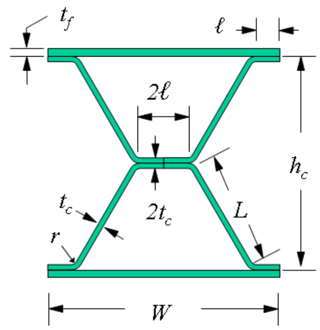

Core Characteristics	
Material	AISI 1010 steel
Height, h_c	5 in
Thickness, t_c	0.125 in
Leg Length, L	2.53 in
Weld Flat Length, ℓ	0.56 in
Corner Radius, r	0.125 in
Width, W	5.4 in
Face Sheet Characteristics	
Material	Domex (100XF) plate
Thickness, t_f	0.25 in for compression panels

In the traditional design of sandwich panels, the properties of interest in the face sheets are high stiffness to provide high flexural rigidity and high tensile and compressive strength. The properties of interest in the core are generally weaker than those in the face sheets. For each sandwich panel in the present study, the face sheet material is Domex (100XF) plate and the core material is American Iron and Steel Institute (AISI) 1010 steel. Domex is a high-strength structural steel that is generally used for applications such as agricultural machinery, crane booms, and railcar components. AISI 1010 steel is a low-strength steel that is typically used for automobile components (e.g., auto bodies and fenders), washers, nails, and rivets.

Although the characteristic material properties of Domex and AISI are consistent with those used in traditional sandwich design for the face sheets and the core, selection of these materials to construct the sandwich panels was not based on design considerations. Rather, these materials were chosen because they were readily available in the desired quantities and thicknesses at the time of construction and scheduling of the tests.

Mechanical properties of the face sheet and core materials were measured from tensile tests conducted on coupons from the same batch of material from which the test panels were constructed. These tensile tests were conducted by Thielsch Engineering, Inc., in Cranston, RI (under contract to CMI), in accordance with standards developed by the American Society for Testing and Materials (ASTM) [15]. The mechanical properties measured in these tests were ultimate tensile strength, 0.2 percent offset yield strength, and elongation over a 1-inch gage length. Moreover, five replicate coupon tests were conducted on each of the five different materials used to construct the sandwich panels in this study. Table 5 lists the results from the tensile tests on the different sandwich panel materials. The values listed in the table represent the average of five tests; the numbers in parentheses are the calculated standard deviation. In subsequent analyses, the compressive and tensile properties of these materials were assumed equal.

Table 5. Tensile Properties of Sandwich Panel Materials

Material	*Ultimate Tensile Strength (ksi)*	*Yield Strength (ksi)*	*Elongation (%)*
Domex plate	113.2 (0.8)	101.2 (1.1)	17.8 (0.3)
AISI 1010 steel 2-in square	71.4 (1.0)	60.5 (2.0)	21.9 (0.4)
AISI 1010 steel 2-in pipe	62.6 (0.4)	52.3 (1.3)	32.2 (0.5)
AISI 1010 steel 3-in pipe	53.6 (0.4)	43.0 (0.6)	35.5 (0.9)
AISI 1010 steel 5-in pipe	51.8 (0.3)	37.1 (1.2)	38.7 (0.9)

Notes:
Values are averages from five tests.
Numbers in parentheses are standard deviations.
Elongation measured over 1-inch gage length.

Pressurized tank cars manufactured since 1989 were built with normalized TC-128B steel.[1] For the sake of comparison, Table 6 lists the minimum requirements for strength and ductility of TC-128B steel.

Table 6. Tensile Property Specifications for TC-128B Steel

Property	*Allowable**
Ultimate Tensile Strength	81–101 ksi
Yield Strength	Greater than 50 ksi
Elongation	Greater than 22%

* AAR Manual of Standards and Recommended Practices and Specifications for Tank Cars, M-1002, Appendix M.

Figure 2 shows the variation of the average yield strength and ultimate tensile strength for the different sandwich panel materials. The error bars in the figure represent the scatter associated with ±2 standard deviations from the mean. The dashed lines represent the nominal properties of 52.9 kilopounds per square inch (ksi) for the ultimate tensile strength and 44.2 ksi for the yield

[1] Prior to 1989, nonnormalized steel was predominantly used. Normalization is a heat treating process that produces a finer and more abundant pearlitic microstructure, which is intended to make the steel stronger and harder compared to non-normalized steel.

strength of AISI 1010 from www.matweb.com. Apparently, the differences between the nominal and actual strength properties can be attributed to cold-forming the shapes of the cores.

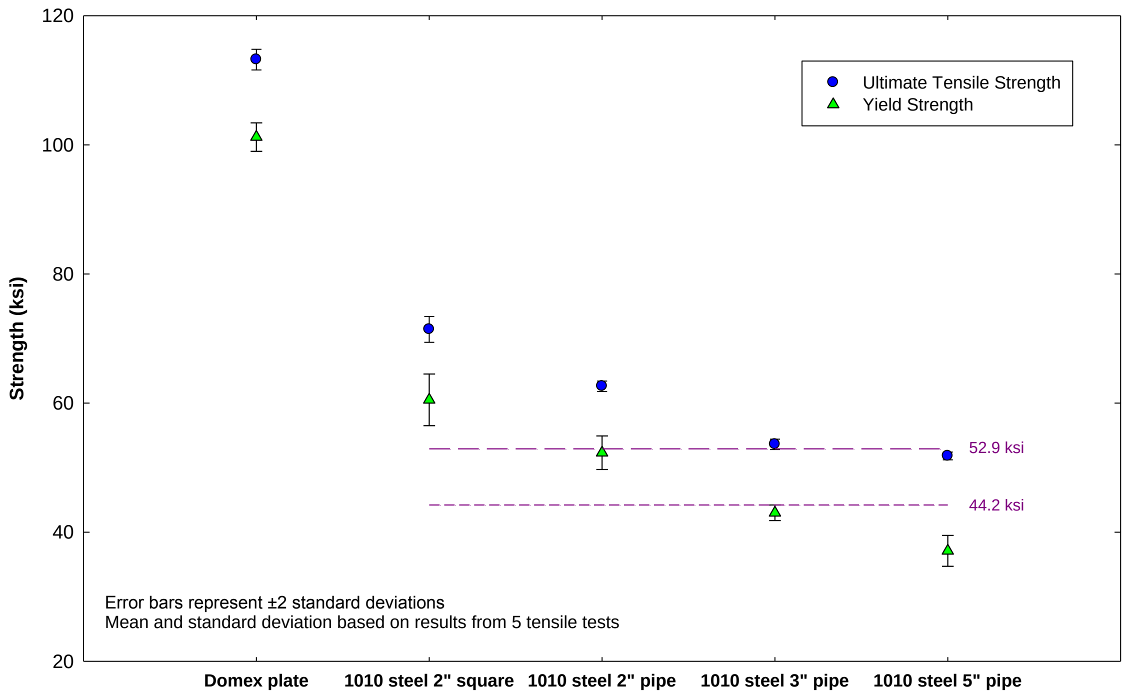

Figure 2. Strength Properties of Sandwich Panel Materials

Similarly, Figure 3 shows the variation and scatter for percent elongation over 1 in for the sandwich panel materials. The figure also shows the nominal value of 20 percent elongation for AISI 1010 from www.matweb.com, which is based on a gage length of about 2 in (50 mm). Elongation is a measure of ductility, which quantifies the ability of the material to deform plastically without fracturing. These figures suggest that for these five materials, strength and ductility are inversely related. Therefore, the material with the highest strength properties (i.e., Domex plate) has the lowest ductility; the material with highest ductility (i.e., AISI 1010 steel 5-inch pipe) has the lowest strength properties.

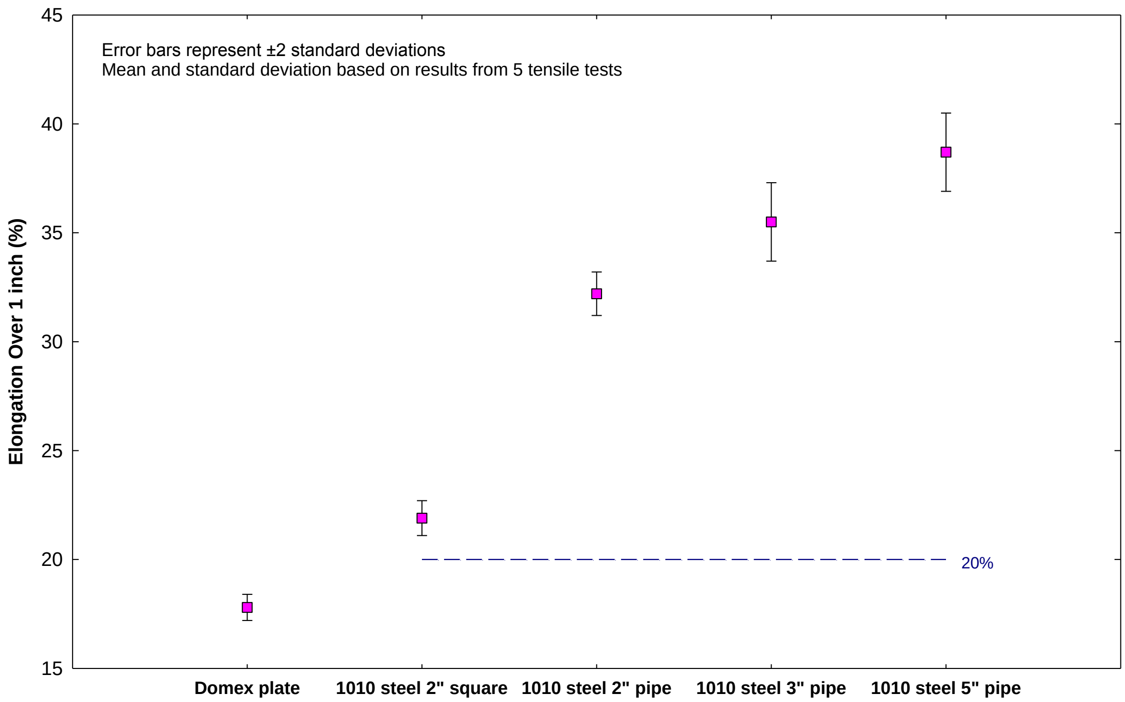

Figure 3. Ductility of Sandwich Panel Materials

The structural characteristics of sandwich structures are often described in terms of relative density. That is, stiffness and strength properties of sandwich panels are commonly reported in relation to core relative density. Core relative density is defined as the ratio of the average density of the core to the density of the material, or equivalently, the volume fraction of the core occupied by the material. The following equations are used to calculate the relative density for the different cores examined in this report:

Pipe Core: $$\rho^* = \frac{\pi t_c \left(D - t_c\right)}{D^2}$$ (refer to Table 2) (1)

Diamond Core: $$\rho^* = \frac{4Lt_c + \pi t_c \left(2r - t_c\right)}{h_c^2}$$ (refer to Table 3) (2)

X-core: $$\rho^* = \frac{4t_c}{h_c W}\left[2\ell + \frac{\pi}{3}\left(2r + t_c\right) + L\right]$$ (refer to Table 4) (3)

Table 7 lists the relative densities for the different cores using these equations and the details of the unit cell dimensions for the individual cores. By comparison, cellular solids such as honeycombs and foams generally have relative densities less than 0.3 [16].[2]

[2] Special ultra-low-density foams can be made with relative density as low as 0.001 [16].

Table 7. Relative Densities for Different Cores

Core Geometry	*Relative Density, ρ**
X-Core	0.075
5-in Pipe Core	0.077
3-in Pipe Core	0.125
Diamond Core	0.131
2-in Pipe Core	0.184

A first-order approximation to calculate relative density of the pipe cores can be calculated using:

$$\rho^* = \frac{\pi t_c}{D} \tag{4}$$

This equation neglects the higher-order terms and tends to overestimate the relative densities calculated by equation (1) and listed in Table 7. The overestimation becomes larger as the outer diameter of the pipe core decreases. For example, the first-order approximation overestimates the relative density of the 5-, 3-, and 2-inch pipe cores by 4.0, 4.8, and 6.5 percent, respectively.

The geometries of the diamond core and the X-core are similar except for the weld flats. If the weld flats in the X-core are ignored, then the geometries are identical. Under this idealized assumption, a first-order approximation to calculate the relative density of both cores can be made from this equation:

$$\rho^* = \frac{2}{\sin\alpha}\left(\frac{t_c}{W}\right) \tag{5}$$

In this equation, α is equal to 45 degrees for the diamond core and 60 degrees for the X-core. In the case of the diamond core, the first-order approximation overestimates the relative density calculated with equation (2) by only 3 percent. The first-order approximation for the X-core, which neglects the presence of the weld flats, underestimates the relative density calculated with equation (3) by more than 20 percent.

In the *Metal Foams Design Guide* [17], core stiffness and strength are normalized by the relative density and material properties as a way to examine and compare different core types or geometries. This normalization practice is adopted in the next section of the report to compare the core strength under uniaxial compression.

3. Behavior under Uniaxial Compression

Tests and analyses were conducted to examine the deformation behavior of flat sandwich panels as a uniform compressive load is applied. The sandwich panels used for test specimens were manufactured by CMI. The crush tests were conducted by ATLSS at Lehigh University's Fritz Engineering Laboratory. The analyses and the test design were performed by the Volpe Center.

Two types of loads are associated with forces impacting sandwich panels: bending and pressure loading. Sandwich panel testing under uniaxial compression is conducted before bend testing because uniform pressure is more basic and simpler to carry out. Testing under this idealized load case examines two components of the sandwich panels: (1) mechanical response or deformation behavior of the core; and (2) strength of the welds. The ultimate mode of failure in sandwich panels subjected to uniaxial compression is the crushing of the core.

Force-crush curves are measured in these tests to characterize the deformation behavior of sandwich panels subjected to uniaxial compression. For sandwich panels with an idealized elastic-perfectly-plastic core material, the force-crush response to uniaxial compression comprises three regimes (see Figure 4): (1) an initial rise in force, (2) a force plateau, and (3) a steep rise in force [16]. Each regime is associated with a different mechanism of deformation. For example, the initial rise in force is representative of linear-elastic material behavior. The force plateau corresponds to plastic deformation or buckling of the core. The steep rise in force is due to densification in which the core is solidly packed together. Two regimes in this idealized force-crush curve are also observed in the compression tests for the cores examined in this report: (1) the initial rise in force representative of linear elasticity; and (2) the densification regime. The shape of the intermediate regime in the force-crush curve depends on the particular core.

For example, Figure 5 shows a trace of a measured force-crush curve from one of the pipe core sandwich panels. The shape of the force-crush characteristic is generally the same for all pipe cores but the force levels associated with the different regimes of the curve depend strongly on the pipe outer diameter.

The initial force rise (i.e., linear-elasticity regime) is followed by a force plateau characteristic of plastic deformation. The plateau is then followed by another rise in force until a local maximum is reached, which is marked in the figure by the solid circle. This local maximum occurs when the deformed shape of the circular cores resembles a rectangle. The vertical legs of the rectangular shape behave as columns, which provide the additional compressive strength above the plateau. The level of the peak force depends on the core height or the pipe diameter. The drop in force after the local maximum signifies plastic collapse or buckling of the core. The force continues to drop until the onset of core densification.

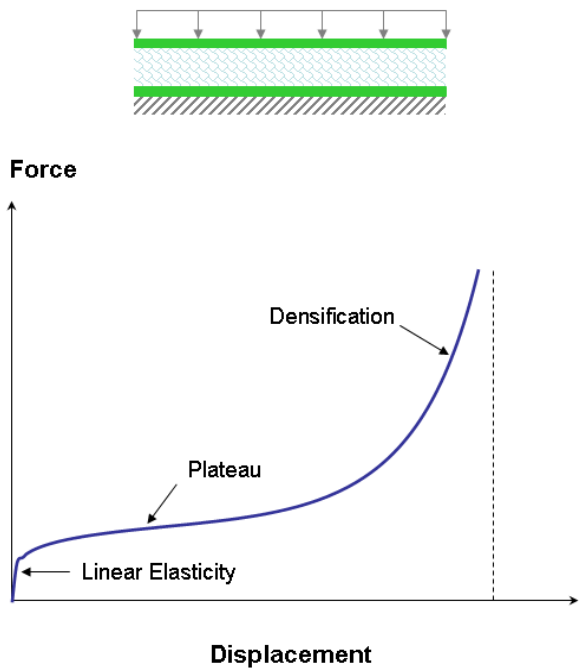

Figure 4. Schematic Force-Crush Response of Sandwich Panel with Idealized Elastic-Plastic Core Material to Uniaxial Compression

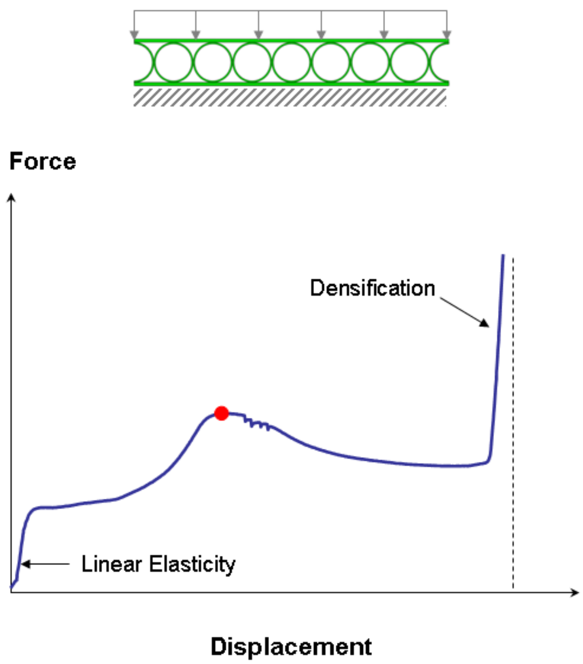

Figure 5. Generic Force-Crush Response of Pipe Core Sandwich Panel

Figure 6 shows a trace from a measured force-crush curve from a diamond core sandwich panel. In this case, the linear-elasticity regime is immediately followed by a rapid drop in force, which represents plastic collapse or buckling of the core. The termination of linear-elasticity regime, which is denoted by the solid circle, coincides with the peak compressive force sustained by the panel. Similarly, Figure 7 shows a trace from a force-crush characteristic measured from one of the X-core sandwich panels. The overall shape of the force-crush characteristic for the X-core is quite similar to that of the diamond core. The similarity in the force-crush response is logical because the diamond core geometry is virtually the same as the X-core without the weld flats. Differences in these two characteristics are evident in the portion of the curves between the peak force and the onset of densification. The diamond core characteristic shows a relatively smooth curve in this regime while the X-core is somewhat jagged. The difference may be attributed to the manner in which the cores were made. The diamond core is a square tube, which is a single part that merely deforms as the core is compressed. The X-core is made from four individual parts that are cold-worked to form the weld flats. The bumps in the jagged curve for the X-core represent deformation of the four welded parts and intermittent tearing of the welds holding them together.

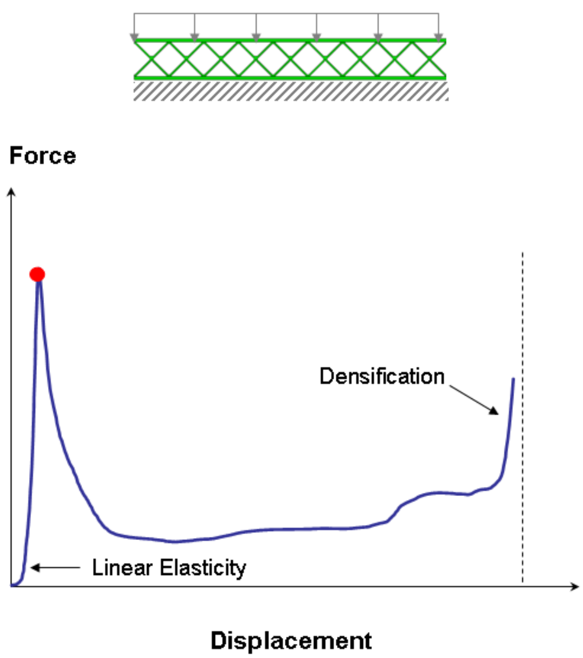

Figure 6. Generic Force-Crush Response of Diamond Core Sandwich Panel

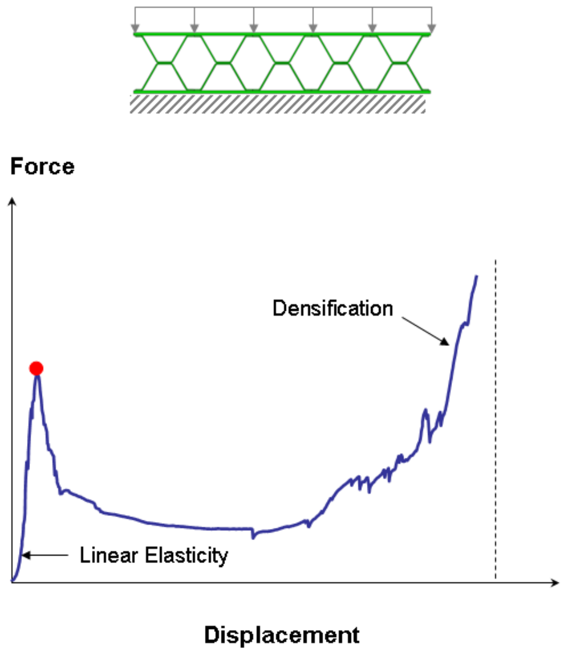

Figure 7. Generic Force-Crush Response of X-Core Sandwich Panel

3.1 Quasi-Static Compression Tests

The test objectives are: (1) to confirm the analytical modeling of sandwich panels; (2) to examine the fabrication issues associated with sandwich panels such as material selection and weld type; (3) to observe the mechanical response or deformation behavior of sandwich panels under uniform pressure; and (4) to rank or prioritize the different cores.

A universal testing machine with a 5-million-pound capacity was used to carry out the uniaxial compression tests. In these tests, quasi-static means that the targeted rate of head travel was 0.2 in per minute.

The matrix for the quasi-static compression tests is given in Table 8, which includes two test variables: (1) core type, and (2) weld type. Generally, the test panel dimensions are 24–27 inches in length by 6 inches in depth. The table includes the weight of each panel, which varied between 33 and 40 pounds depending on the core. Other details such as dimensions and materials used for the face sheets and the cores are described in Section 2. The force-crush curves measured during the 14 quasi-static compression tests are shown in Appendix A. The peak loads, as depicted in the schematic force-crush characteristics for each core, are determined from these curves and are also listed in Table 8.

Table 8. Quasi-Static Compression Test Matrix

Test Order	Serial Number	Core Type	Panel Length	Panel Depth (in)	Panel Weight (lb)	Weld Type	Peak Load (kip)
1	0047-01	5-in pipe core	5 cores 25"	6	36.5	Slot/skip (Manual)	38
2	0047-03	3-in pipe core	8 cores 24"	6	33.9	Slot/skip (Manual)	128
3	0047-05	2-in pipe core	12 cores 24"	6	34.3	Slot/skip (Manual)	273
4	0047-07	2-in pipe core	12 cores 24"	6	34.2	Slot/skip & stitch between core elements (manual)	615
5	0047-14	Diamond core	9 cores 24"	6	33.4	Slot/skip & stitch between core elements (robotic)	420
6	0047-09	X-core	5 hats 27"	6	40.0	Spot (manual)	52
7	0047-11	X-core	5 hats 27"	6	40.0	Slot & spot (manual)	53
8	0047-02	5-in pipe core	5 cores 25"	6	36.4	Slot/skip (robotic)	37
9	0047-04	3-in pipe core	8 cores 24"	6	33.8	Slot/skip (robotic)	126
10	0047-06	2-in pipe core	12 cores 24"	6	34.3	Slot/skip (robotic)	458
11	0047-08	2-in pipe core	12 cores 24"	6	34.3	Slot/skip & stitch between core elements (robotic)	628
12	0047-13	Diamond core	9 cores 24"	6	33.1	Slot & skip (robotic)	398
13	0047-10	X-core	5 hats 27"	6	40.0	Spot (manual)	62
14	0047-12	X-core	5 hats 27"	6	40.0	Slot & spot (robotic)	75

A normalization procedure adopted from the *Metal Foams Design Guide* [17] is used in this report to compare the compressive strength of different cores. Moreover, compressive strength is characterized by a nondimensional quantity, $\sigma_{peak}/\sigma_o\rho^*$. Peak compressive stress, σ_{peak} is the peak load (from Table 8) divided by the loaded cross-sectional area of the panel (generally approximately 144 square inch (in^2) or 1 ft^2). Nondimensional compressive strength is peak compressive stress divided by yield strength of the core material, σ_o (from Table 5) and relative density, ρ^* (from Table 7).

Figure 8 shows a log-log plot of nondimensional compressive strength as a function of relative density. In this plot, attributes of an optimal design would be low relative density (implying light weight) and high strength. The figure shows that the nondimensional compressive strength of the cores examined in this report is correlated to relative density. Cores with the lowest relative densities, namely, the 5-inch pipe core and the X-core, have the lowest compressive strengths. Conversely, cores with the highest relative densities (the diamond core and the 2-inch pipe core) have the highest compressive strengths. Because the correlation does not trend toward an optimal design, a trade-off between strength and core density (i.e., weight) must be made to select the most favorable cores from the five that were tested. For example, the 2-inch pipe core exhibits the highest strength, but sandwich panels made with such cores may be too heavy and might require more welding than is practical for the intended application. The diamond core and the 3-inch pipe core appear to be reasonable alternatives that may provide adequate structural performance within weight constraints and are used in the bend tests (which are described in the next section of this report).

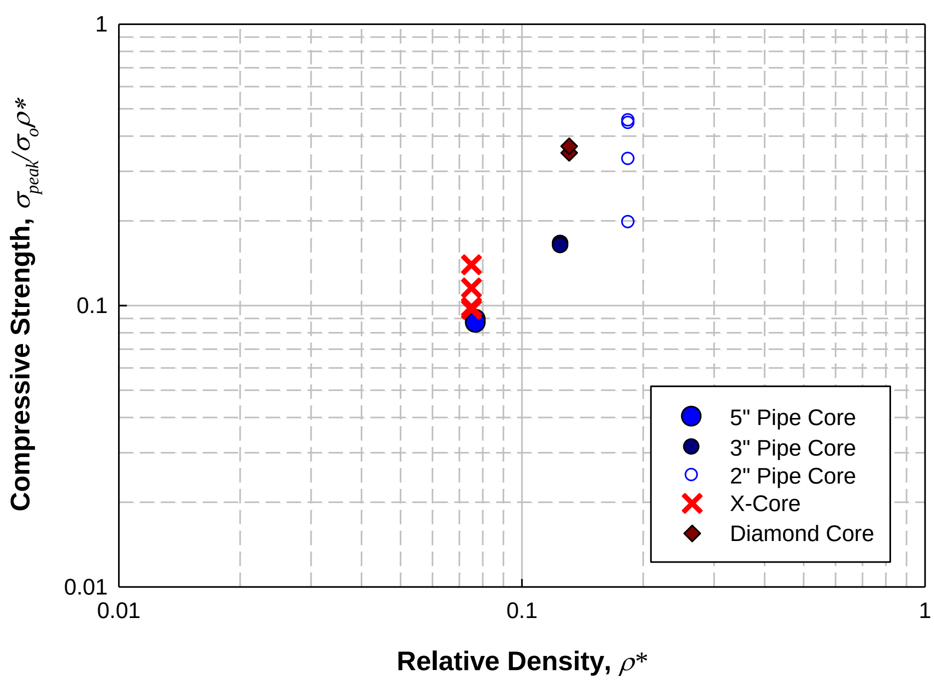

Figure 8. Variation of Compressive Strength with Relative Density

Figure 8 shows a variation in strength for the 2-inch pipe cores. The highest level of compressive strength for the 2-inch pipe core corresponds to the panel in which the core elements are welded to each other at the 3- and 9-o'clock positions. Compressive strength is reduced when the cores are not welded to each other at these horizontal locations. Similarly, the figure shows a variation in strength for the X-cores, although this variation is less than that for the 2-inch pipe cores. In the case of the X-cores, the highest strength is from the panel that was slot and spot welded robotically. Whereas, the lowest strength is from a panel that was spot welded manually.

3.2 Comparisons with Analysis

Analytical and computational methods are applied to examine the strength and deformation behavior of sandwich panels under compression. Analytical methods are based on the assumption of elastic-perfectly-plastic material behavior. Calculations based on finite element analysis account for strain hardening effects. Results from these methods are used to design the quasi-static tests and to interpret test results.

Analytical methods based on plastic limit load analysis [18, 19] are applied to estimate the strength (and stiffness) of sandwich structures. Limit analysis is well established for estimating collapse loads under the assumption of elastic-perfectly-plastic material behavior. The following equation is derived from limit analysis to estimate the compressive strength of the pipe core sandwich panels:

$$\frac{\sigma_{peak}}{\sigma_o \rho^*} = \frac{2.56}{\rho^*}\left[1 - \sqrt{1 - \frac{4}{\pi}\rho^*}\right]^2 \qquad (6)$$

where σ_o is the yield strength of the core material and ρ^* is the relative density. Specific details to derive this equation are described in Appendix B.

Figure 9 compares the nondimensional compressive strength measured in the pipe cores to the theoretical estimate based on limit analysis. The figure shows excellent agreement between the measured strength and the closed-form equation.

A similar equation can be derived from limit load analysis to estimate the compressive strength of the diamond core sandwich panels:

$$\frac{\sigma_{peak}}{\sigma_o \rho^*} = 0.5 \qquad (7)$$

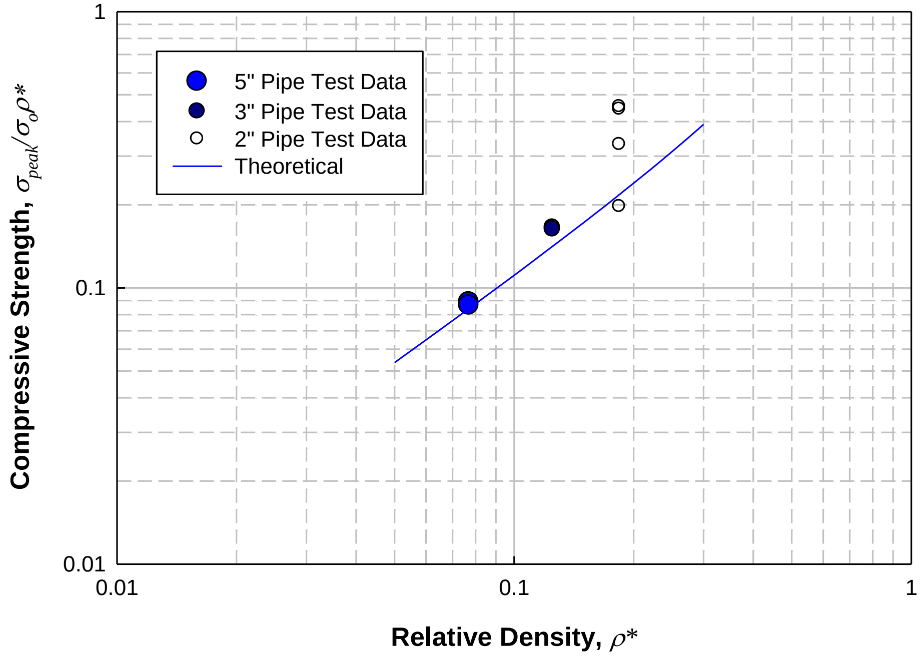

Figure 9. Variation of Theoretical and Measured Strength of Pipe Cores with Relative Density

Figure 10 compares the nondimensional compressive strength from the measurements of the diamond core sandwich panels with the theoretical estimate. In this case, however, the analytical equation overpredicts the measured data by more than 40 percent. The discrepancy is due to the differences in the assumed and actual core geometries. The analytical equation is based on the idealized assumption that the diamond core is a perfect square, whereas the actual core has rounded corners (see Table 3). Because the legs of the diamond are somewhat curved and not perfectly straight, plastic collapse of the core initiates at a lower force level than would be expected under the idealized geometry.

Finite element calculations are performed using the general-purpose finite element package ABAQUS. The face sheets and the cores of the sandwich panels are modeled using linear shell elements. Finite element analysis produces qualitatively similar force-crush characteristics as those measured in the quasi-static compression tests. However, the force levels in the finite element results are generally higher than the test data at the same levels of displacements. For example, Figure 11 shows a comparison between the measured and the posttest calculated force-crush curves for the 5-inch pipe core. In the present context, “posttest” means that the materials properties used in the finite element calculations were those measured from the tensile tests that were reported in Section 2. The comparison shown in the figure is typical of the qualitative agreement in the shape of the measured and calculated curves for all cores, but is also representative of higher force levels calculated by the finite element analysis. The overestimation is due to neglect of manufacturing imperfections and the assumption of perfect geometry. The sensitivity of finite element predictions to imperfections was discovered in previous work on diamond lattices [12].

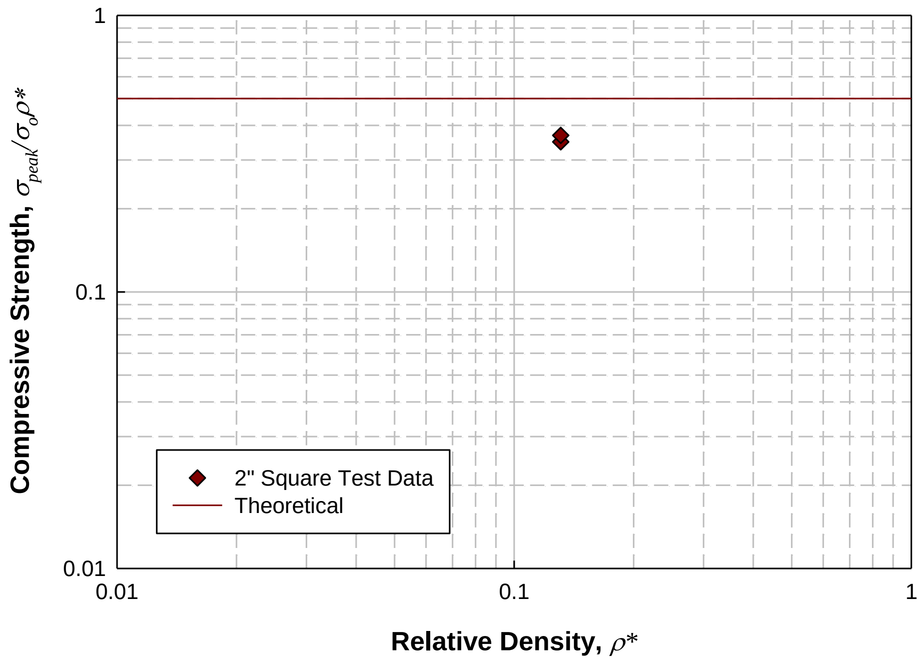

Figure 10. Variation of Theoretical and Measured Strength of Diamond Core with Relative Density

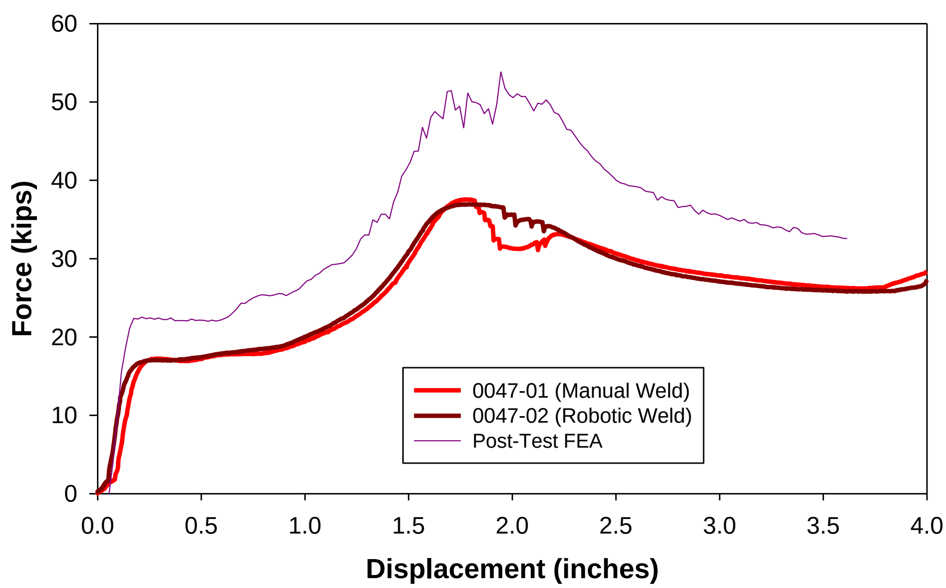

Figure 11. Measured and Calculated Force-Crush Curves for 5-Inch Pipe Core

Deformation patterns for different cores from finite element analysis resemble the observed deformation behavior. For example, Figure 12 shows a comparison of the deformation predicted from the finite element analysis at four levels of crush and video clips from the quasi-static compression test at the same levels of crush. The predicted deformation patterns are similar to the observed modes. The predicted deformations are based on finite element analyses performed prior to conducting the tests and before the actual mechanical properties of the materials were measured.

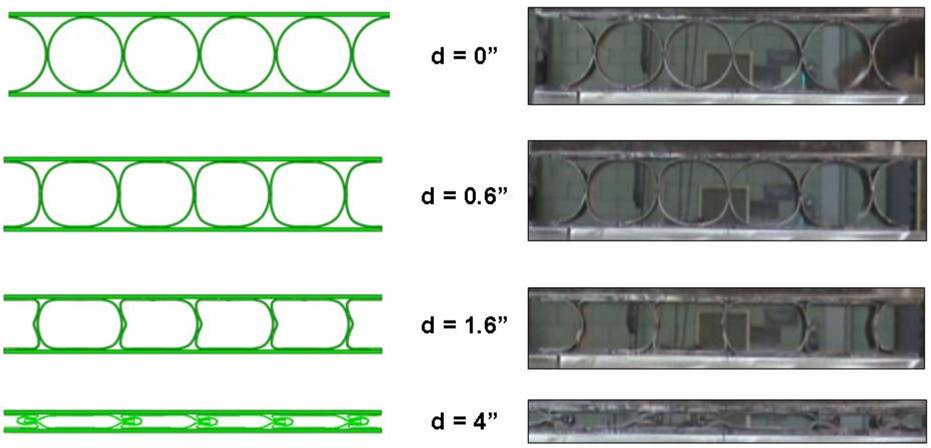

Figure 12. Predicted and Observed Deformation of 5-Inch Pipe Core

Figure 13 compares a close-up view of the predicted (left) and observed (right) deformation in a single pipe core at 4 in of crush. The test for this particular panel was terminated at this point. Moreover, the details of the deformation pattern at this level of crush are remarkably similar.

Figure 13. Closeup View of Final Deformation Mode in 5-Inch Pipe Core

4. Behavior under Bending with an Indenter

Similar tests and analyses were conducted to examine the deformation behavior of welded steel sandwich panels under bending by using an indenter to transmit load. The quasi-static bend tests were also conducted at Lehigh University's Fritz Engineering Laboratory by using the 5-million-pound capacity universal machine that was used in the compression tests. In the bend tests, local collapse modes of the sandwich panels were examined in addition to the force-displacement behavior.

Results from the uniaxial compression tests were used in designing the bend tests. Of the five cores examined previously in the uniaxial compression tests, two were selected for bend testing: the 3-inch pipe core and the 2-inch square diamond core. The face sheets were made using the same material (Domex plate) as the compression tests, but the thickness was reduced from 0.25 to 0.118 in, which reduced the overall panel weight.

Figure 14 shows a schematic of the bend test configuration. Bending load was applied to the sandwich panels using a 12- by 12-inch indenter with rounded (1-inch radius) edges. The panels were simply supported over solid, 4-inch diameter round bars with a center-to-center span of 24 in. The round bars were welded onto a virtually rigid (i.e., very stiff) platen. The overall length of the sandwich panels used in the bend tests was typically 48 in. Therefore, each end of the sandwich panels has about a 12-inch overhang. After about 4 in of indenter travel, the sandwich panel contacts the rigid platen. Additional crushing of the core after this point was similar to that observed in the previous compression tests. The sequence of loading, such as panel bending followed by crushing of the core, was similar to that in an idealized tank car impact scenario where the panel must bend and crush to protect the commodity-carrying tank.

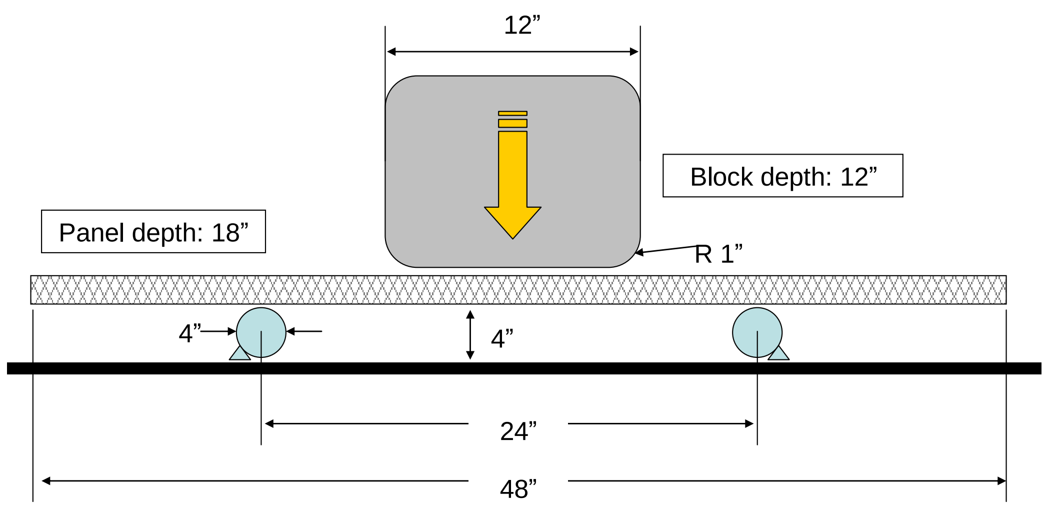

Figure 14. Schematic of Bend Test Configuration

Figure 15 shows the general shape of the expected force-displacement response in the bend tests. The schematic exhibits three phases of panel deformation. The first phase of the curve is an initial rise in force, representative of elastic bending. The second phase initiates when a local collapse mode is engaged. The particular local collapse mechanism depends on several factors such as span length, face sheet and core characteristics (e.g., dimensions, material properties, and geometry), and indenter characteristics (e.g., size and shape). These local collapse mechanisms are discussed in the next section of this report. The schematic characterizes the local collapse phase as a force plateau, but in some cases, the response may actually exhibit a softening behavior (i.e., a drop in force). Softening occurs when the relative distance between the face sheets decreases as the core compresses, which effectively reduces the bending inertia and decreases the moment and, therefore, the load carried by the panel. The third phase of deformation starts when the indenter travel is approximately equal to the roller support diameter, and the bottom of the sandwich panel comes into contact with the rigid platen. During the compression phase, the deformation of the sandwich panel is similar to that observed in the uniaxial compression tests.

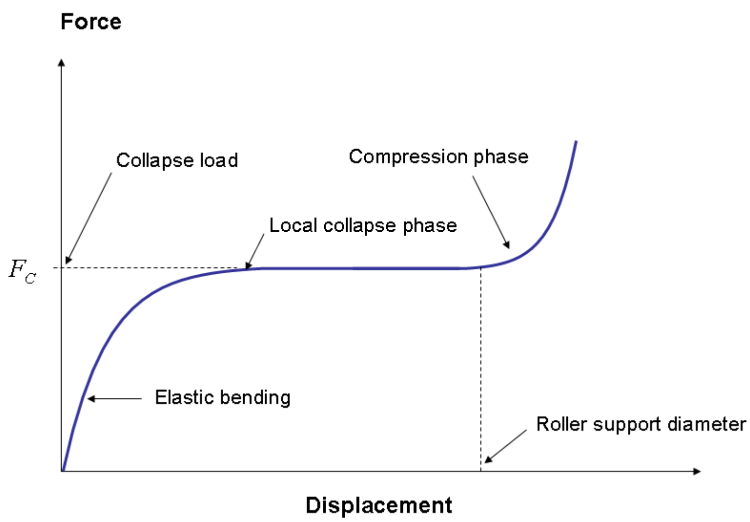

Figure 15. Schematic Force-Displacement Curve in Bend Test

One of the factors affecting the force level that characterizes the local collapse phase (denoted as F_C in Figure 15) is bending direction. The bending strength of the panel depends on the orientation of the cores with respect to the axis of bending. Moreover, the dependence of strength on core orientation means that bending behavior is anisotropic. Referring to the test configuration shown in Figure 14, the cores in the bend test panels were aligned either perpendicular or parallel to the supports. Panel bending strength is expected to be higher when the cores are perpendicular to the supports compared to when the cores are parallel to the supports.

4.1 Local Collapse Modes

The collapse mode of sandwich panels under uniaxial compression is crushing of the core. However, sandwich panels subjected to bending with an indenter can collapse locally in several ways. Three local collapse modes of sandwich panels in bending, which are shown schematically in Figure 16, are (1) face sheet yield or fracture, (2) local indentation, and (3) core shear.

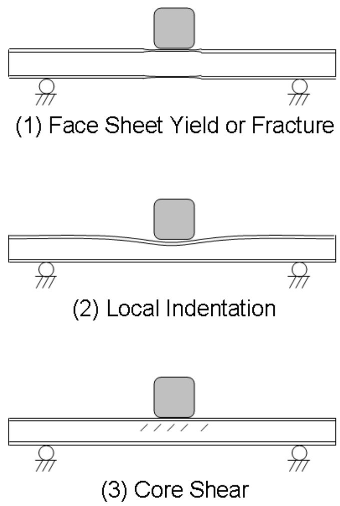

Figure 16. Possible Local Collapse Modes in Bending

For a panel undergoing bending in the test configuration, the stress state in the top face sheet is compressive while that in the bottom face sheet is tensile. As the load transmitted through the indenter increases, plastic hinges may form at the edges of the indenter when the deformations become plastic. At sufficiently large deformations, the stress state in the top face sheet may also become tensile. Moreover, local failure of the face sheets may occur if the compressive or tensile stresses are high enough to cause yielding or fracture.

Local indentation may occur when the face sheet comes in contact with the indenter and acts as a plate on an elastic-plastic support provided by the core. In this case, the top face sheet bends independently of the opposite (or bottom) face sheet. If the stress applied to the core exceeds its compressive strength, the core will collapse.

In short-span panels under three-point bending, the core is mainly subjected to shear stresses and carries most of the transverse force. Core failure may occur if the shear stress exceeds the shear strength of the core material. In long-span panels, normal stresses in the core can be of the same order of magnitude or even higher than the shear stresses. In this case, the core is subjected to biaxial stresses and core failure may occur if the effective transverse shear stress exceeds the shear strength of the core material.

Previous research has been conducted to examine the concept of a collapse mechanism map that describes how various factors affect the initiation of different local collapse modes [17, 20–22]. These factors include characteristics of the core and the face sheets (i.e., material properties, geometry, and dimensions), span length, and indenter size. For example, the *Metal Foams Design Guide* [17] provides analytical equations to calculate the collapse loads associated with the three modes shown in Figure 16 based on the assumptions of perfectly-plastic material behavior and three-point bending applied through a flat-bottomed indenter. The collapse loads for the three modes are plotted on a diagram with nondimensional axes of core height divided by span length and core thickness divided by core height.

Figure 17 shows a diagram developed for a 3-inch pipe core panel with characteristics provided in

Table 2 and assuming a 12-inch indenter with a simply-supported span length of 24 in. The solid circle in the diagram indicates that failure of the 3-inch pipe core panel is likely to occur from local collapse due to excessive shear stresses in the core.

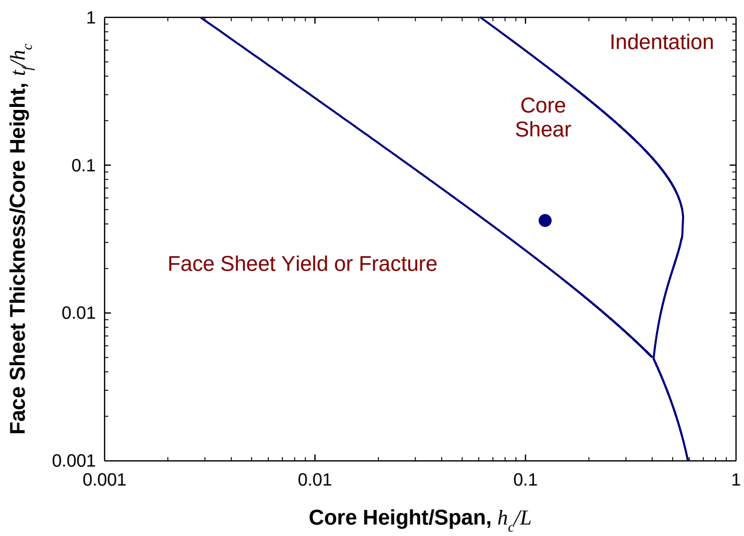

Figure 17. Collapse Mechanism Map for 3-Inch Pipe Core Panel in Bending

Figure 18 shows a similarly constructed collapse mechanism map for the diamond core panel. In this case, the core height (see Table 3) is slightly smaller than the pipe core (2.62 vs. 3 in). The change in core dimensions relative to span length and face sheet thickness alters the local collapse mode from core shear to face sheet yield or fracture. Results from the compression tests are used to construct the collapse mechanism maps for the two different cores. In both cases, the collapse mechanism maps indicate that face sheet yield or fracture is likely to occur in panels with relatively thin face sheets (i.e., small values of t_f/h_c) and in relatively long panels (i.e., small values of h_c/L). Core shear is generally expected to occur in the panels in the present bend tests. The collapse mechanism map shown in Figure 18; however, suggests that face sheet yield or fracture may also be expected to occur in some cases with the diamond core panels.

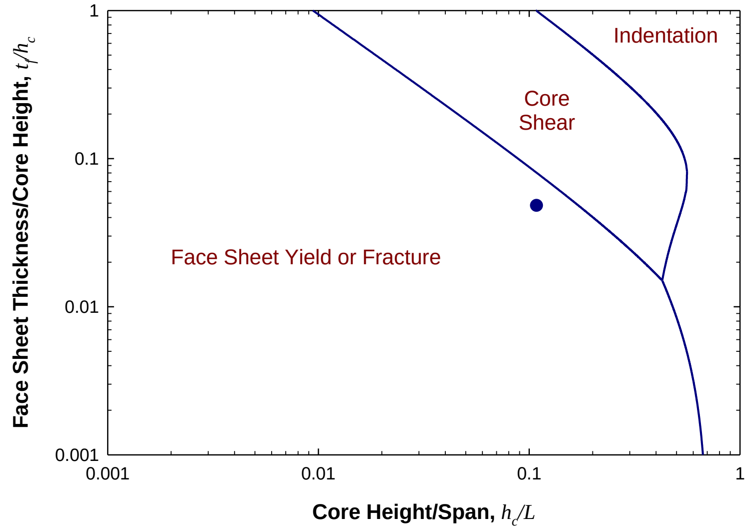

Figure 18. Collapse Mechanism Map for Diamond Core Panel in Bending

Interestingly, fracture of the bottom face sheet occurred during the quasi-static bend tests with both diamond core panels with solid face sheets and cores oriented perpendicular to the supports. Figure 19 shows the extent of cracking between welds in the bottom face sheet of one panel. Moreover, the face sheet fracture corresponds to the local failure mode indicated by the collapse mechanism map for the diamond core panels in Figure 18.

Figure 19. Photograph of Face Sheet Fracture from Quasi-Static Bend Test

In traditional sandwich design, panels that are efficient in absorbing energy are also stiff. For panels with the attributes of high strength and stiffness, in-plane tension in the face sheets increases the likelihood of local failure by yielding, tearing, or fracturing. Finite element simulations have shown a rapid decrease in panel effectiveness once local failure of the face sheets occurs. To mitigate the likelihood of engaging this local failure mode, the concept of strip face sheets was introduced as a variable in the test matrix for the bend tests. Simulations also confirm that using strips relieves in-plane tension in the face sheets, and may help distribute the applied load over a larger area.

A quick and inexpensive method was conceived to quantify load spreading during some of the quasi-static bend tests. A sheet of plastic bubble wrap was taped to the rigid platen between the roller supports before conducting the test. As bending loads were applied through the indenter, the bottom face sheet eventually came into contact with the platen. At this point, the protruding air-filled hemispheres in the bubble wrap were squeezed and “popped.” After the test was completed, the boundaries of popped bubbles on the sheet that outlined the contact area, such as the area of load spreading, were examined.

The bubble wrap method was used to measure load spreading in two bend tests. In both tests, the sandwich panels were made with solid face sheets and cores running parallel to the supports. One test involved a pipe core sandwich in which the boundaries of the contact area were measured as 16 inches in the direction of the supports by 14.5 inches in the direction perpendicular to the supports. The other test involved a diamond core panel, where the corresponding measurements were 16 by 13.25 in. Sixteen inches was the total width for the particular brand of bubble wrap that was used in these tests. Therefore, the actual amount of load spreading along the direction of the parallel cores may be even greater. On the basis of these two measurements, the sandwich panels distributed load over an area that is conservatively estimated to be 50–60 percent greater than the indenter footprint (12 by 12 in). Figure 20 shows the bend test configuration with the bubble wrap as the pipe core sandwich panel is bending.

Figure 20. Bend Test with Bubble Wrap to Quantify Load Spreading

4.2 Quasi-Static Bend Tests

The objectives of the quasi-static bend tests were as follows: (1) to confirm the analytical and computational modeling of sandwich panels and (2) to observe the mechanical response of the sandwich panels under bending. The observation of mechanical response includes measuring the force-displacement behavior and indentifying the local collapse modes which were previously described in Section 4.1.

Table 9 shows the test matrix for the quasi-static bend tests in which three test variables are evident: (1) core geometry (3-inch pipe core and 2-inch square diamond core), (2) core orientation relative to the rollers used to support the panel (cores running either parallel or perpendicular to the supports), and (3) face sheet type (solid plates on both sides, strips used as face sheets on both sides, and a combination of the two). In the present bend tests, quasi-static means that the indenter was lowered onto each of the sandwich panels at a rate of approximately one-quarter inch per minute.

The term "hybrid" is used in this report to refer to the face sheet type where a solid plate is attached to one side of the sandwich panel and strips are used on the opposite side. In the test matrix, Serial Number 0047-29 is called Hybrid A in which strips are placed on top and a solid face plate is on the bottom in the test fixture. Serial Number 0047-30 is called Hybrid B in which the placement of the face sheets with respect to the indenter is reversed (i.e., solid plate on top, strips on bottom). Both hybrid panels are constructed with diamond cores that are aligned perpendicular to the supports.

Appendix C is a compendium of the 16 force-displacement (i.e., distance of head travel) curves measured during the bend tests. These curves are used to estimate the collapse load as shown in Figure 15. The local collapse loads are plotted in Figure 21 in ascending order for each panel. Moreover, the collapse loads are used as a measure to quantify the relative effect of the test variables. In some cases, the collapse load is distinct, and is read directly from the force-displacement curve as the local maximum value within the local collapse phase. In other cases, particularly for panels with cores aligned parallel to the supports, no local maximum is evident. In these cases, the collapse load is considered as the force level at which the compression phase appears to initiate. Generally, this occurs after about 4 in of displacement, when the bottom of the panel comes into contact with the very stiff platen.

Figure 21 clearly indicates that the bending strength of the panels used in this test series is strongly anisotropic. Panels with cores perpendicular to the supports are much stronger in bending than those with cores parallel to the supports. The collapse load for the perpendicular core panels is about five (for pipes) to six (diamonds) times that of the corresponding parallel core panels.

For solid face sheets, the collapse loads for the diamond core panels were slightly higher on average (about 15 percent) than those for the pipe core, independent of the core orientation. For strip face sheets, the collapse loads for both cores were nearly the same.

Table 9. Quasi-Static Bend Test Matrix

Test Order	Serial Number	Core Type	Core Orientation Relative to Supports	Face Sheet Type	Panel Length	Panel Depth	Panel Weight (lb)	Weld Type
1	0047-19	3-in Pipe	Parallel	Solid	16 cells 48”	18”	139.5	Manual
2	0047-15	Diamond	Parallel	Solid	18 cells 47.2”	18”	139.5	Manual
3	0047-26	3-in Pipe	Parallel	Strip	16 cells 48”	18”	111.0	Robotic
4	0047-24	Diamond	Parallel	Strip	47.2”	7 cells 18.34”	111.5	Robotic
5	0047-21	3-in Pipe	Perpendicular	Solid	48”	6 cells 18”	141.0	Manual
6	0047-17	Diamond	Perpendicular	Solid	47.2”	7 cells 18.34”	140.0	Manual
7	0047-25	3-in Pipe	Perpendicular	Strip	48”	6 cells 18”	110.5	Robotic
8	0047-23	Diamond	Perpendicular	Strip	47.2”	7 cells 18.34”	109.5	Robotic
9	0047-29	Diamond	Perpendicular	Solid & strip	47.2”	7 cells 18.34”	126.0	Manual
10	0047-20	3-in Pipe	Parallel	Solid	16 cells 48”	18”	139.5	Robotic
11	0047-16	Diamond	Parallel	Solid	18 cells 47.2”	18”	139.5	Robotic
12	0047-28	Diamond	Parallel	Strip	18 cells 47.2”	18”	109.0	Manual
13	0047-22	3-in Pipe	Perpendicular	Solid	48”	6 cells 18”	142.5	Robotic
14	0047-18	Diamond	Perpendicular	Solid	47.2”	7 cells 18.34”	137.0	Robotic
15	0047-27	Diamond	Perpendicular	Strip	47.2”	7 cells 18.34”	110.0	Manual
16	0047-30	Diamond	Perpendicular	Solid & strip	47.2”	7 cells 18.34”	126.0	Manual

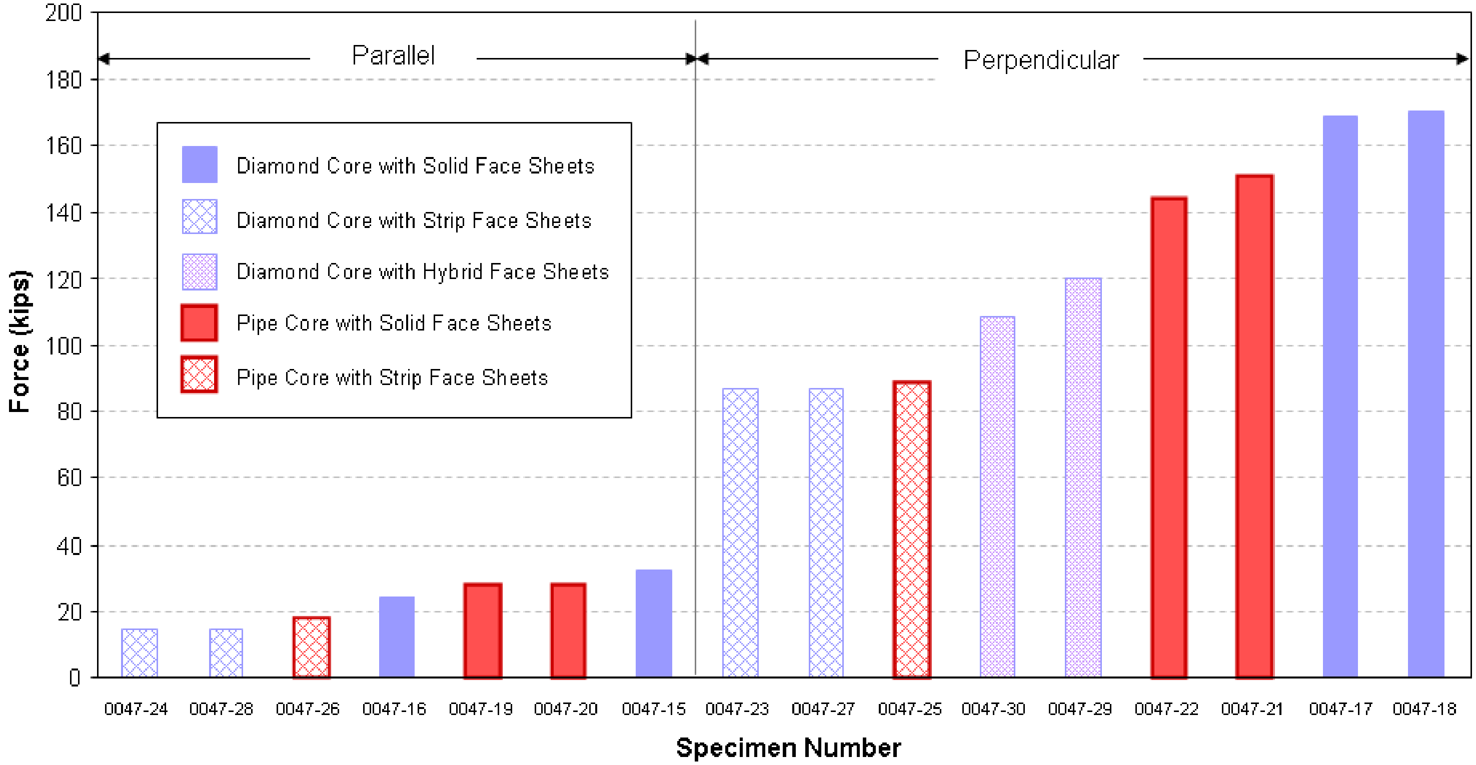

Figure 21. Collapse Loads in Bend Tests

Panels with solid face sheets are stronger in bending than those with strips. The difference in the collapse loads is between 35 and 49 percent depending on the particular configuration. The differences are slightly greater for the diamond cores (42–49 percent) compared to the pipe cores (35–40 percent).

The force-displacement behavior for the two hybrid panels is nearly the same before the compression phase. The collapse load for Hybrid A is approximately 10 percent higher than that for Hybrid B.

The two panels exhibiting the largest collapse loads are the replicate diamond core panels with solid face sheets and cores oriented perpendicular to the supports (i.e., strong-bending direction). In the test matrix (Table 9), these panels correspond to Serial Numbers 0047-17 and 0047-18. Cracks between welds were observed in the bottom face sheets of both panels.

The general-purpose finite element package ABAQUS/Explicit was used to carry out calculations to predict the force-displacement response of the sandwich panels in the bend tests. The pretest predictions from the finite element analysis are included in the compendium of force-displacement curves given in Appendix C. The predictions are generally higher than the measured responses. Again, the discrepancy in overpredicting strength is attributed to the neglect of manufacturing imperfections in the analyses, which was seen in the comparisons in the compression tests and in the previous work on diamond lattices [12].

5. Summary of Test and Analysis Results

Observations and results from the tests and analyses of sandwich panels subjected to quasi-static uniaxial compression are summarized as follows:

1. Tests on panels with similar cores and weld types exhibit excellent repeatability.

2. Compressive strength is correlated to relative density. Compressive strength increases as relative density increases. The 2-inch pipe cores provide the highest compressive strength but also have the highest relative density.

3. Strength estimates for the pipe cores based on plastic limit load analysis are in excellent agreement with measured compressive strength. Similar analytical estimates for the diamond cores are more than 40 percent higher than the measured data. The discrepancy may be attributed to the idealized assumptions regarding the geometry (i.e., perfectly square diamond core) and material (i.e., elastic-perfectly-plastic) behavior.

4. Finite element analysis produces force-crush curves that are in good agreement with those measured in the tests. The finite element analysis results generally overestimate strength, which may be attributed to the neglect of manufacturing imperfections.

5. Deformation modes simulated by finite element analysis resemble those observed in the tests.

Observations and results from the tests and analyses of sandwich panels subjected to quasi-static bending using an indenter are summarized as follows:

1. Tests on panels with similar cores and weld types exhibit excellent repeatability.

2. Bending strength of the sandwich panels is strongly anisotropic. Panels with cores perpendicular to the supports are much stronger in bending than those with cores parallel to the supports. Collapse loads for perpendicular core panels are five (for pipes) to six (diamonds) times those for the parallel core panels.

3. Replacing solid face sheets with strip face sheets reduces panel bending strength by approximately 35–49 percent.

4. Cracking in the bottom face sheet was observed in the two diamond core panels with cores perpendicular to the supports using solid face sheets. Cracking was not obvious in the diamond core panels with the same orientation using strip face sheets. On the basis of these results, it appears that the use of strip face sheets may mitigate the onset of face sheet yield or fracture.

5. The force-displacement behavior for both hybrid panels is nearly the same before the compression phase. The collapse load for Hybrid A (i.e., strip face sheets on top, solid plate

on bottom) is approximately 10 percent higher than that for Hybrid B (solid plate on top, strip face sheets on bottom).

6. Force-displacement (i.e., indenter travel) curves calculated by finite element analysis overpredict the force level compared to the test data in every case, but are within reasonable agreement. The discrepancy is attributed to modeling perfect geometry, whereas imperfections likely exist in actual test panels. The sensitivity of finite element analysis to imperfections was also found in previous testing and computational analysis of sandwich panels with stainless steel diamond lattices [12].

6. Discussion

Previous research identified sandwich structures as a potential technology that could improve the crashworthiness of commodity-carrying tank cars [6–8]. One of the concepts currently under development treats the pressurized commodity-carrying tank as a protected entity using sandwich structures as protective panels in the event of an accident. Two critical advantages for using sandwich structures in traditional design applications are: (1) sandwich structures are known to provide greater flexural stiffness and strength than those of a solid plate of equal mass; and (2) material arrangement in the core can add functionality such as thermal insulation and energy absorption.

The energy-absorption capability makes sandwich structures attractive as a means to protect railroad tank cars during crashes. In theory, protective sandwich panels under impact would absorb the kinetic energy of the moving object. Energy-absorption requirements for generalized tank car head and shell impact scenarios have been estimated by calculating kinetic energy [25]. The kinetic energy associated with the impact of two fully loaded tank cars (each weighing 286,000 lb) with a closing speed of 25 miles per hour (mph) is 6 million ft-lb. For a closing speed of 30 mph, the kinetic energy is 8.6 million ft-lb. However, absorbing energy levels of this magnitude is a formidable challenge because the design of such a system is constrained by the maximum allowable weight and clearance standards for rail cars. The effect of weight and space budgets on improved designs is discussed in previous work [7].

Finite element simulations to model sandwiches as protective panels during impact are ongoing. These models incorporate results from the engineering studies described in this report on mechanical behavior under compressive and bending loads. Force-displacement curves from these simulations, however, do not differ significantly from those of a conventional tank car impact without protective panels. Such results indicate that the levels of energy absorbed by sandwich panels are relatively small compared to the kinetic energies corresponding to impact closing speeds of 25 and 30 mph. Moreover, the results suggest that, due to weight and space limitations, the structural rigidity of the commodity-carrying tank must be integrated with the sandwich panels in order to absorb more kinetic energy than the protective panels alone.

The simulation results further suggest that the primary benefit of using sandwich structures in the protection concept is gained from their ability to distribute load over a larger area of the tank with respect to the indenter footprint (i.e., load blunting). The bubble wrap method described in Section 4 indicates that sandwich panels can distribute the load over an area that is at least 50–60 percent greater than the indenter footprint. These estimates of the contact area are conservative because an indenter with a footprint of 12 by 12 in is assumed. Because the edges of the indenter are rounded with a 1-inch radius, the footprint may be considered to be 10 by 10 in. In this case, the increased contact area becomes 116–132 percent larger than the indenter footprint. Whereas, requirements for energy absorption are readily determined from a calculation of kinetic energy; it is unclear how to determine an appropriate target for load spreading. It is also unclear whether or not a contact area that is 1.5 or 2.3 times that of the indenter footprint is sufficient to prevent puncture in a tank covered by a sandwich panel as an effective shield. Additional research may be needed to better understand the mechanics of load spreading offered by protective panels.

Finite element analysis reveals the following sequence of events that typically occurs when a sandwich panel cannot protect the commodity-carrying tank against puncture from an indenter. The face sheet initially impacted by the indenter fails by fracture. Failure of this outer face sheet is followed by core failure, which in turn is followed by failure of the inner face sheet, and then puncture of the tank. Moreover, once failure in the outer face sheet occurs, global failure of the sandwich and the commodity-carrying tank is imminent.

The finite element analysis also indicated that failure of the face sheets is inherently due to excessive in-plane tension. Therefore, design features that can reduce or mitigate the effect of in-plane tension in the face sheets will help to maintain the integrity of the sandwich structure under impact and to enable its load-spreading functionality. For example, the detrimental effect of in-plane tension was demonstrated in the quasi-static bend tests using diamond core panels with solid face sheets and cores oriented in the strong bending direction (i.e., perpendicular to the supports). But when the sandwich design was modified by using strips rather than solid face sheets, local failure of the bottom face sheet by fracture was preempted. In-plane tension is also influenced by the boundary conditions of the panel or the manner in which the panel is supported. Another concept to mitigate this effect is to employ relatively small panels or tiles as a protective layer rather than a larger continuous cover. Additional research is needed to explore this concept.

All sandwich panels used in the compression and bend tests described in this report were constructed with equal thickness face sheets. Finite element models were also used to examine the concept of using unequal thickness face sheets. Preliminary results indicate that thickening the outer face sheet delays the time to initiate failure, but the failure rate actually increases rapidly through the protective panels once it initiates in the core. Thickening the inner or bottom face sheet allows more time for the core to completely fail. Therefore, it appears that increasing the thickness of the bottom face sheet is more effective in protecting the tank than increasing the thickness of the top face sheet. This inference is supported by the fact that the sandwich panels that failed in the quasi-static bend tests exhibited cracking in the bottom face sheet.

Structural behavior and functionality of sandwich panels depends strongly on the core arrangement and the relative density. Figure 22 compares the nondimensional compressive strength of the cores examined in the present study with data extracted from other studies on stainless steel corrugated cores [12], stainless steel diamond lattices [12], aluminum alloy metal foams [17], stainless steel square honeycombs [23], and stainless steel pyramidal truss cores [24]. The dashed lines through the extracted data represent best-fit curves whereas the solid line through the pipe core data is the theoretical estimate based on limit analysis from equation (6). The figure indicates that the cores examined in this report (namely the pipe, diamond, and X-cores) exhibited lower compressive strength than the square honeycomb, pyramidal truss, and corrugated cores. Conversely, the cores in this report exhibited greater strength than aluminum alloy foam.

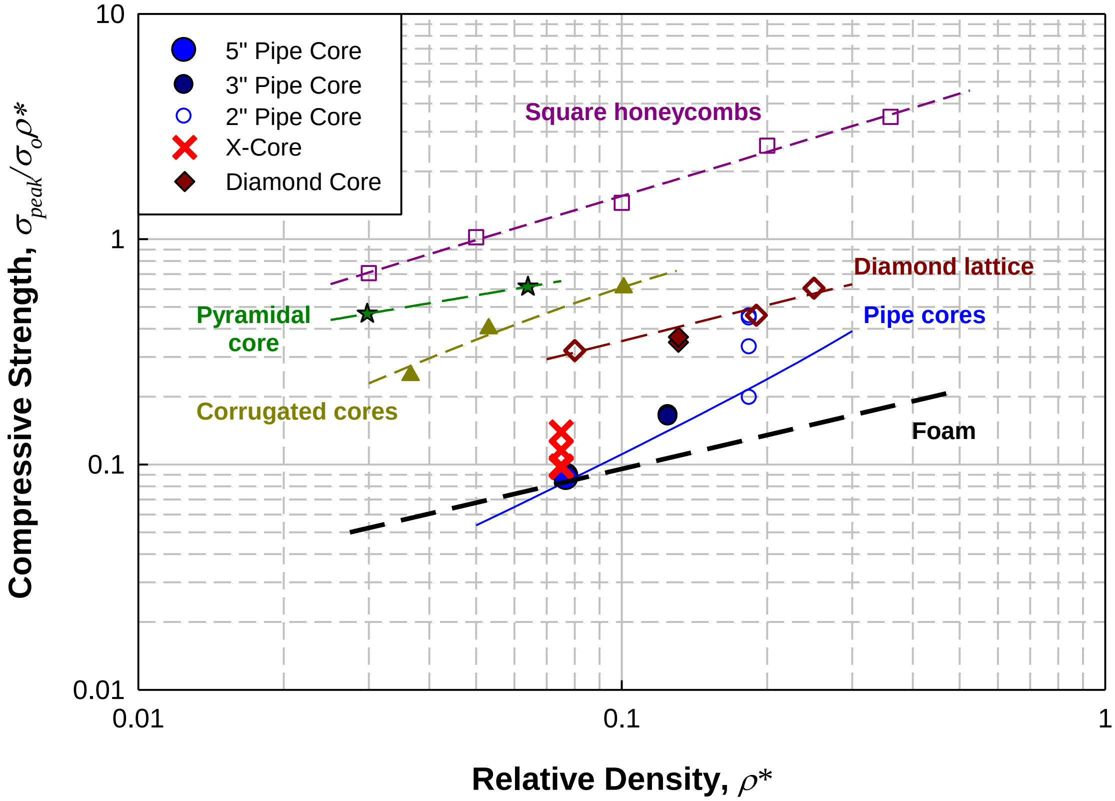

Figure 22. Comparison of Compressive Strength for Different Cores

Clearly, several options exist for selecting core shape or geometry for optimal design. In traditional sandwich design, high strength and stiffness are attributes of an optimal design. In the concept of a protection system against puncture from an indenter; however, it is unclear whether these attributes are desirable. Stiffer panels imply more strength, but finite element simulations suggest that such panels are more vulnerable to face sheet tearing due to excessive in-plane tension as described previously.

The materials used to construct the sandwich panels for the compression and bend tests were not varied. The selection of these materials was based on current availability of the desired quantities and thicknesses when tests were being planned. Moreover, the specific details of the sandwich panels as described in Section 2 do not represent optimal designs for structural performance. Preliminary finite element simulations of generalized tank car impacts suggest that an optimal design might employ materials with high-strength properties in the face sheets and high ductility in the cores.

The basic research described in this report examined certain fabrication issues. For example, in previous work sponsored by the Office of Naval Research [12], diamond lattice materials were manufactured as cores of sandwich panels by slotting together stainless steel sheets and then brazing together the assembly. In the present study, off-the-shelf (OTS) tubes (circular tubes for the pipe cores and square tubes for the diamond cores) were welded to the face sheets to construct sandwich panels. Figure 22 also shows that the nondimensional compressive strength of the diamond cores in the present study is slightly lower than the regression curve for the diamond lattices assembled with the slotting and brazing technique. The different construction methods may explain the variation in compressive strength, but this is not significant.

The quasi-static compression and bend tests included replicate panels to examine potential differences due to welding procedures (e.g., manual versus robotic). The results indicate that the variability in structural performance is almost negligible in the replicate panels. Therefore, the combination of using OTS tubing for circular pipes and square diamonds and joining them together with the various welding procedures provides repeatability in structural performance.

Results from the quasi-static tests and analyses described in this report indicate that overall performance of sandwich panels is strongly sensitive to imperfections. The imperfection sensitivity of sandwich structures confirms similar results from previous work [12, 26]. In the present study, imperfections were considered in terms of imperfect geometry. However, flaws or defects may develop during the fabrication process that can degrade performance. The potential for such imperfections may introduce an issue of quality control if construction of sandwich structures for the current application becomes viable.

Obviously, the quasi-static tests described in this report do not account for dynamic effects on deformation behavior. Two separate effects should be distinguished in the context of dynamic response of structures: strain rate and impact velocity. Strain rate effect is a material property in which the effective yield strength increases as the strain rate is raised. The latter effect is material inertia that leads to enhanced stresses during impact, which may affect the mechanism of local collapse. Understanding the development of local collapse mechanisms that evolve to global failure is critical in assessing the structural performance of sandwich structures as protective panels, and is a major objective of the present work. The next logical step for ongoing research would be to design and implement a dynamic impact test to examine inertial effects. Moreover, additional research is needed to reach the ultimate goal of demonstrating the performance of a candidate protective system against puncture from an indenter carrying sufficient weight.

7. References

[1] National Transportation Safety Board. (2004). "Derailment of Canadian Pacific Railway Freight Train 292-16 and Subsequent Release of Anhydrous Ammonia Near Minot, North Dakota January 18, 2002," Railroad Accident Report NTSB/RAR-04/01.

[2] Nayak, P. R., Rosenfield, D. B., and Hagopian, J. H. (1983). "Event Probabilities and Impact Zones for Hazardous Materials Accidents on Railroads," Final Report, DOT/FRA/ORD-83/20.

[3] Anderson, R. T., and Barkan, C.P. (2004). Railroad accident rates for use in transportation risk analysis. *Transportation Research Record*, *1863,* 88–98.

[4] Treichel, T. T. (2007). "Specific Locations of Damage and Lading Losses on Tank Heads and Shells," RSI-AAR Railroad Tank Car Safety Research and Test Project Report No. RA 06-04.

[5] Jeong, D. Y., Tang, Y. H, Yu, H., Lyons, M. L., Gordon, J. E., Orringer, O., and Perlman, A. B. (2009). "Engineering Studies on Structural Integrity of Railroad Tank Cars Under Accident Loading Conditions," Final Report, DOT/FRA/ORD-09/18.

[6] Tyrell, D. C., Jeong, D. Y., Jacobsen, K., and Martinez, E. (2007). "Improved Tank Car Safety Research," *Proceedings of the 2007 ASME Rail Transportation Division Fall Technical Conference*, RTDF2007-46013.

[7] Tyrell, D. C., Jacobsen, K., Talamini, B., and Carolan, M. (2007). "Developing Strategies for Maintaining Tank Car Integrity During Train Accidents," *Proceedings of the 2007 ASME Rail Transportation Division Fall Technical Conference,* RTDF2007-46015.

[8] Carolan, M., Talamini, B., and Tyrell, D. C. (2008). "Update on Ongoing Tank Car Crashworthiness Research: Predicted Performance and Fabrication Approach," *Proceedings of the 2008 IEEE/ASME Joint Rail Conference*, JRC2008-63052.

[9] Carney, J. F., III, Dougan, C. E., Hargrave, M. W. (1985). "The Connecticut Impact Attenuation System," Application of Safety Appurtenances, Transportation Research Board, *Transportation Research Record*, *1024*, 41–50.

[10] Carney, J. F., III. (1989). "The Connecticut Narrow Hazard Crash Cushion," Design and Testing of Roadside Safety Devices, Transportation Research Board, *Transportation Research Record*, *1233*, 43–50.

[11] Alghamdi, A. A. A. (2001). Collapsible impact energy absorbers: an overview. *Thin-Walled Structures, 39,* 189–213.

[12] Côté, F., Deshpande, V. S., Fleck, N. A., and Evans, A. G. (2006). The compressive and shear responses of corrugated and diamond lattice materials. *International Journal of Solids and Structures*, *43*, 6220–6242.

[13] Wei, Z., Deshpande, V. S., Evans, A. G., Dharmasena, K. P., Queheillalt, D. T., Wadley, H. N. G., Murty, Y. V., Elzey, R. K., Dudt, P., Chen, Y., Knight, D., and Kiddy, K. (2008). The resistance of metallic plates to localized impulse. *Journal of the Mechanics and Physics of Solids*, *56*, 2074–2091.

[14] Wadley, H. N., Fleck, N. A., and Evans, A. G. (2003). Fabrication and structural performance of periodic cellular metal sandwich structures. *Composites Science and Technology*, *63*, 2331–2343.

[15] ASTM Standard A370. (2003). "Standard Test Methods and Definitions for Mechanical Testing of Steel Products," West Conshohocken, PA: ASTM International, www.astm.org.

[16] Gibson, L. J., and Ashby, M. F. (1997). *Cellular Solids: Structure and Properties*, 2nd edition, Cambridge University Press.

[17] Ashby, M. F., Evans, A., Fleck, N. A., Gibson, L. J., Hutchinson, J. W., and Wadley, H.N.G. (2000). *Metal Foams: A Design Guide*, Washington, DC: Butterworth-Heinemann.

[18] Chakrabarty, J. (1988). *Theory of Plasticity*, 2nd edition, London: McGraw-Hill.

[19] Lubliner, J. (2008). *Plasticity Theory*, New York: Dover Publications Inc.

[20] Triantafillou, T. C., and Gibson, L. J. (1987). Failure mode maps for foam core sandwich beams. *Materials Science and Engineering*, *95*, 37–53.

[21] Petras, A., and Sutcliffe, M. P. (1999). Failure mode maps for honeycomb sandwich panels. *Composite Structures*, *44*, 237–252.

[22] Tagarielli, V. L., and Fleck, N.A. (2005). A comparison of the structural response of clamped and simply supported sandwich beams with aluminum faces and a metal foam core. *Journal of Applied Mechanics*, *72*, 408–417.

[23] Côté, F., Deshpande, V. S., Fleck, N. A., and Evans, A. G. (2004). The out-of-plane compressive behavior of metallic honeycombs. *Material Science Engineering A*, *380,* 272–280.

[24] Zok, F. W., Waltner, S. A., Wei, Z., Rathbun, H. J., McKeeking, R. M., and Evans, A. G. (2004). A protocol for characterizing the structural performance of metallic sandwich panels: application to pyramidal truss core. *International Journal of Solids and Structures*, *41*, 6249–6271.

[25] Jeong, D. Y., Tyrell, D. C., Carolan, M. E., and Perlman, A. B. (2009). "Improved Tank Car Design Development: Ongoing Studies on Sandwich Structures," *Proceedings of the 2009 ASME Joint Rail Conference*, JRC2009-63025.

[26] Biagi, R., and Bart-Smith, H. (2007). Imperfection sensitivity of pyramidal core sandwich structures. *International Journal of Solids and Structures, 44*, 4690–4706.

Appendix A. Force-Crush Curves from Compression Tests

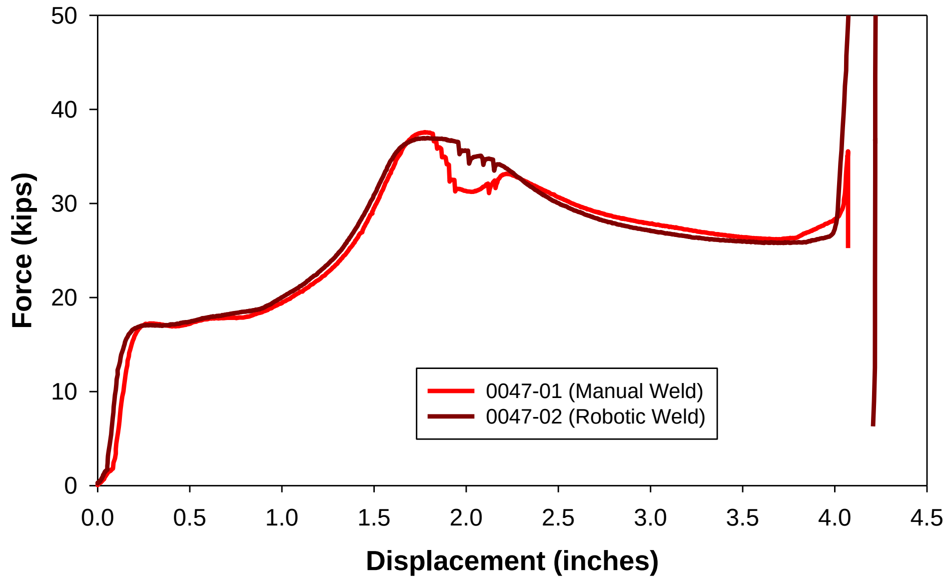

Figure A1. Measured Force-Crush Curves for 5-Inch Pipe Cores

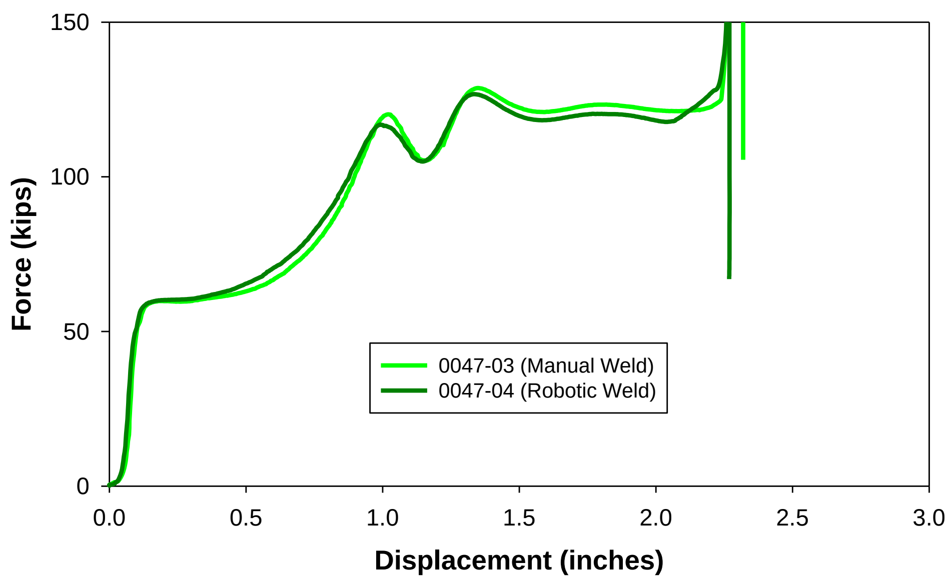

Figure A2. Measured Force-Crush Curves for 3-Inch Pipe Cores

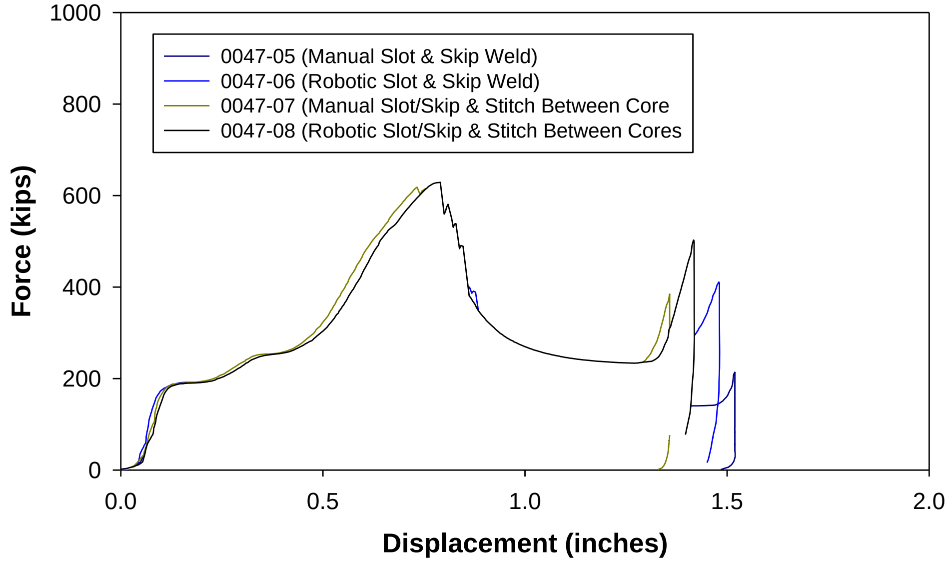

Figure A3. Measured Force-Crush Curves for 2-Inch Pipe Cores

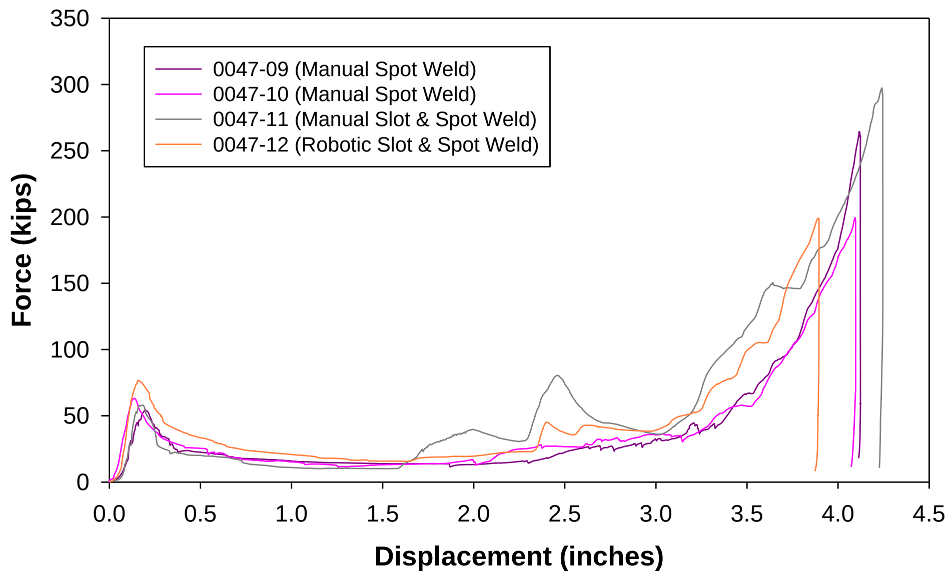

Figure A4. Measured Force-Crush Curves for X-Cores

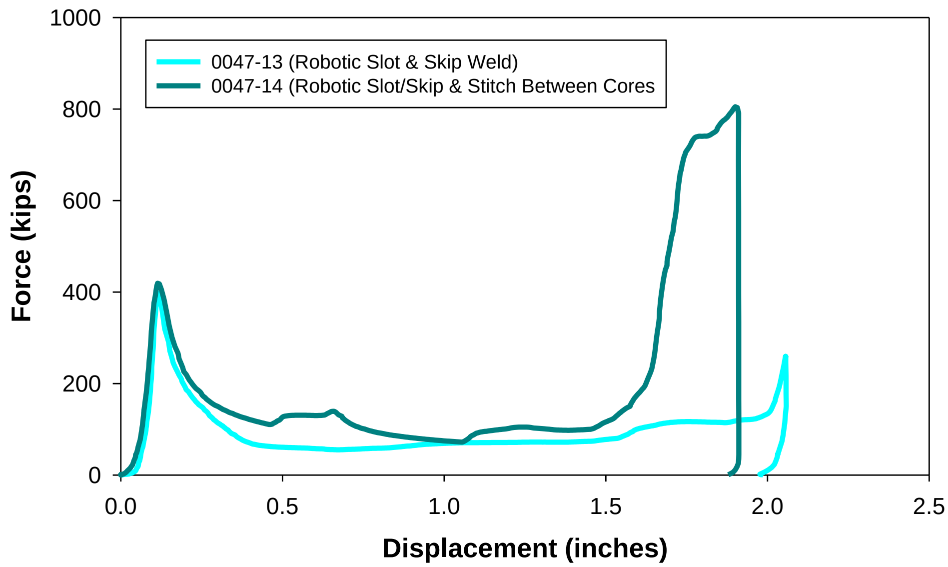

Figure A5. Measured Force-Crush Curves for Diamond Cores

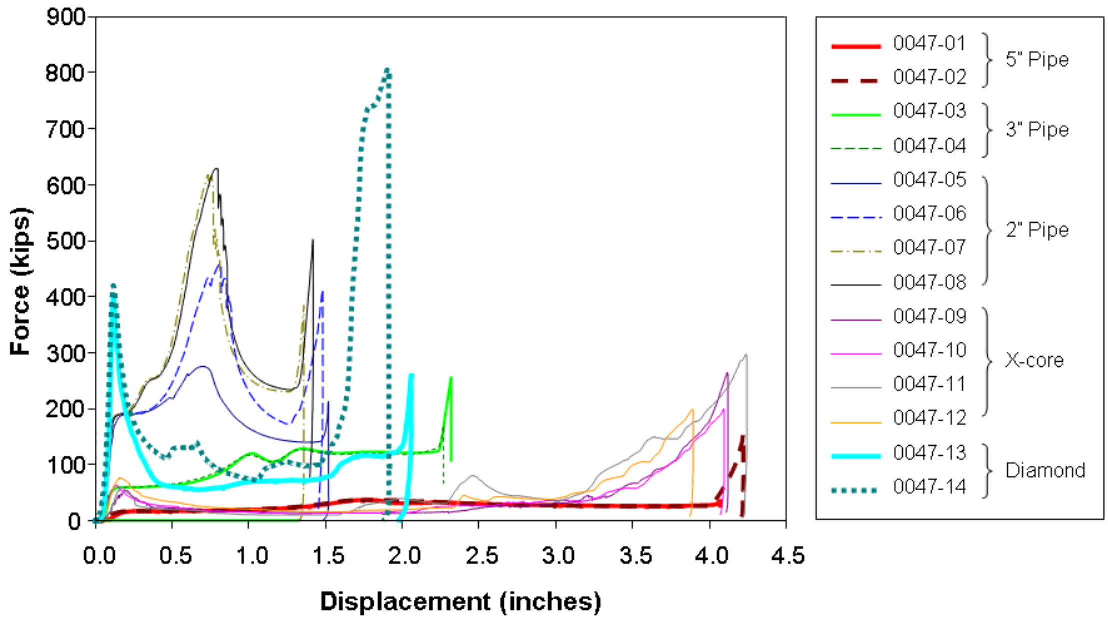

Figure A6. Measured Force-Crush Curves for All Cores

Appendix B. Estimation of Core Strength by Limit Analysis

Analytical methods are applied to estimate the plastic collapse loads for the pipe and diamond cores under a compressive load. Moreover, these analytical methods are based on the theory of plastic limit analysis [18, 19]. Estimates of plastic collapse load are compared with the measurements obtained from the quasi-static compression tests that were conducted at Lehigh University.

B.1 Pipe Core Estimates

Figure B1 shows the geometry of a flat sandwich panel with two pipes with diameter *D* in its core.

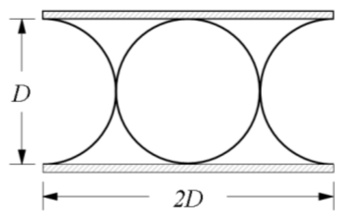

Figure B1. Sandwich Panel with Pipe Core

Under compressive loading, the upper half of the center pipe in the sandwich cell shown in Figure B2 is assumed to behave in a similar manner as a semicircular arch with pinned supports subjected to an equivalent concentrated load (Figure B3):

$$P = \sigma_2 \cdot D \cdot b \qquad \text{(B-1)}$$

where σ_2 is the compressive stress, *D* is the outer diameter of the pipe, and *b* is the depth of the panel.

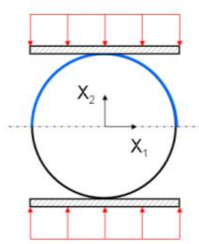

Figure B2. Sandwich Cell under Compression

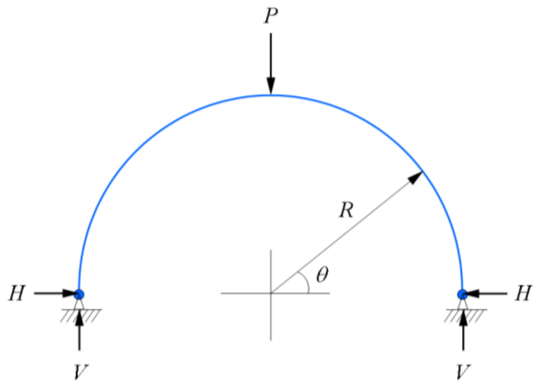

Figure B3. Semicircular Arch with Pinned Ends

The vertical reaction load at the pinned supports, V is found from equilibrium, while the horizontal reaction load, H is determined from applying Castigliano's theorem:

$$V = \frac{P}{2} \tag{B-2}$$

$$H = \frac{P}{\pi} \tag{B-3}$$

As the semicircular arch deforms plastically, hinges are assumed to form at the locations shown schematically in Figure B4. One hinge is assumed to develop directly under the centrally applied load. Hinges are also assumed to form at the pinned supports. In addition, hinges are assumed to develop at the location of maximum negative (hogging) bending moment, which is characterized in Figure B4 by the rotational angle θ_o.

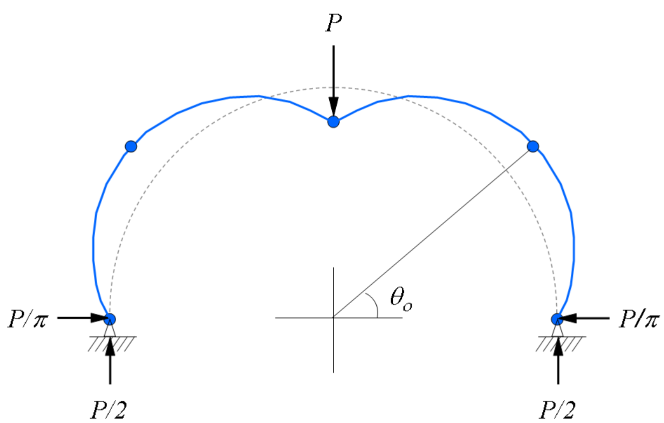

Figure B4. Arch Mechanism at Plastic Collapse

Considering only the right half of the semicircular arch shown in Figure B3, the bending moment as a function of the rotational angle, θ is given by

$$M(\theta) = VR(1-\cos\theta) - HR\sin\theta = PR\left[\frac{1}{2}(1-\cos\theta) - \frac{1}{\pi}\sin\theta\right] \quad 0 \le \theta \le \frac{\pi}{2} \tag{B-4}$$

where R is the radius of the semicircular arch. The derivative of this equation with respect to θ is

$$\frac{\partial M}{\partial \theta} = PR\left(\frac{1}{2}\sin\theta - \frac{1}{\pi}\cos\theta\right). \tag{B-5}$$

The angle at which the maximum hogging moment occurs is determined by setting this derivative equal to zero, from which

$$\theta_o = \tan^{-1}\left(\frac{2}{\pi}\right) = 32.5^o. \tag{B-6}$$

The maximum hogging moment is

$$M(\theta_o) = \frac{PR}{2\pi}\left(\pi - \sqrt{\pi^2+4}\right) = -0.093PR. \tag{B-7}$$

The absolute value of this moment is used in the remainder of this derivation. The plastic collapse load is determined from equating this maximum moment to the fully plastic moment

$$M_o = \frac{1}{4}\sigma_o t^2 b \tag{B-8}$$

where σ_o is the yield strength of the core material and t is the thickness of the pipe. Therefore, the compressive strength of the pipe core may be expressed in terms of its material yield strength and geometric parameters as follows

$$\frac{\sigma_2}{\sigma_o} = \frac{\pi}{4}\left(\pi + \sqrt{\pi^2+4}\right)\left(\frac{t}{D}\right)^2 = 5.39\left(\frac{t}{D}\right)^2. \tag{B-9}$$

Alternatively, a similar equation for plastic collapse of the pipe core may be derived from assuming a different type of collapse mechanism. In this method, the collapse mechanism is assumed to consist of a polygon inscribing the circular pipe. Figure B5 shows a schematic of the collapse mechanism in the shape of an octagon.

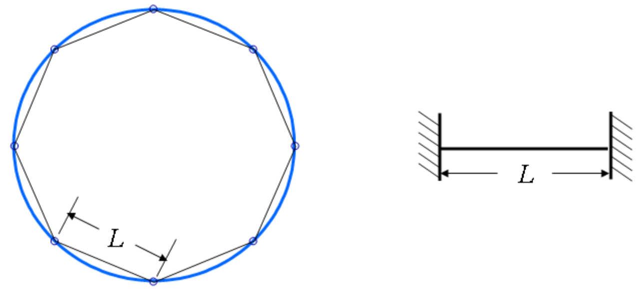

Figure B5. Collapse Mechanism for Circular Pipe

Moreover, each side of the polygon is assumed to behave as a fixed-end beam, which the collapse load is calculated from

$$P_o = \frac{8M_o}{L} \tag{B-10}$$

where L is the equivalent length of the beams. For a polygon of equal-length sides, the equivalent beam length is calculated from

$$L = D\sin\frac{\pi}{n} \tag{B-11}$$

where n is the number of sides to the polygon (which is also equal to the number of hinges). Therefore, an approximate expression for the collapse load of the pipe core can be derived as:

$$\frac{\sigma_2}{\sigma_o} = \frac{2}{\sin\frac{\pi}{n}}\left(\frac{t}{D}\right)^2 \tag{B-12}$$

For n equal to 8,

$$\frac{\sigma_2}{\sigma_o} = 5.23\left(\frac{t}{D}\right)^2 \tag{B-13}$$

which is about 3 percent lower than equation (B-9), derived from the semicircular arch mechanism.

The plastic collapse loads associated with the sandwich panels used in the quasi-static compression tests are calculated from:

$$P_C = \frac{2\sigma_o}{\sin\frac{\pi}{n}}\left(\frac{t}{D}\right)^2 \cdot A \qquad \text{(B-14)}$$

where A is the loaded cross-sectional area of the panel.

Table B1 lists the outer diameter, the measured tensile yield strength, and the loaded cross-sectional area for the tested sandwich panels with pipe cores. Yield strengths are the averages of tensile test measurements on five different samples of AISI 1010 steel from the same batch used to construct the test articles. The core thickness was the same for each panel, and was equal to 0.125 in. Table B1 also compares the calculated plastic collapse load using equation (B-14) and assuming eight links (i.e., n=8) with measurements for the initial collapse load. Figure B6 compares the calculated and measured collapse loads corresponding to the initial peak for the three pipe diameters.

Table B1. Plastic Collapse Estimates and Initial Peak Observed in Tests on Pipe Cores

D (inch)	σ_o (ksi)	A (in^2)	P_C (kip) Calculated (n = 8)	P_C (kip) Test
2	52.3	144	154	190
3	43.0	144	56	60
5	37.1	150	18	17

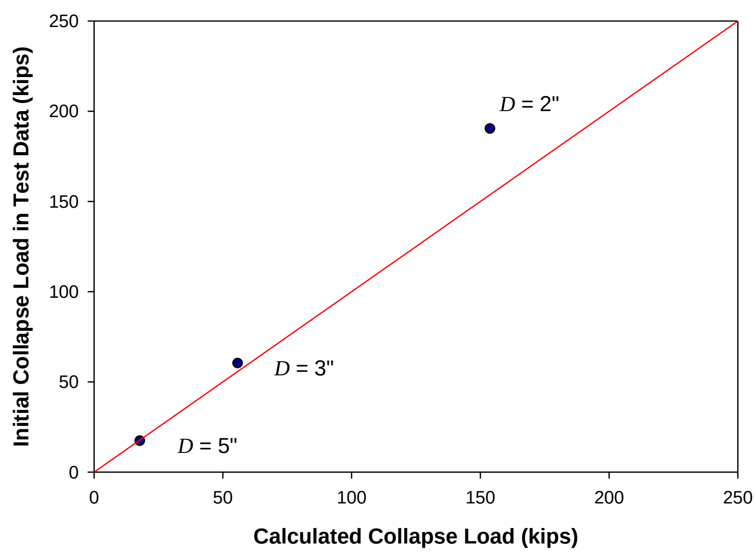

Figure B6. Comparison of Calculated and Measured Initial Peak Loads

On the basis of videos and finite element simulations of the quasi-static compression tests, the initial plastic collapse load appears to occur when the pipe deforms into a shape resembling a square, as shown in Figure B7.

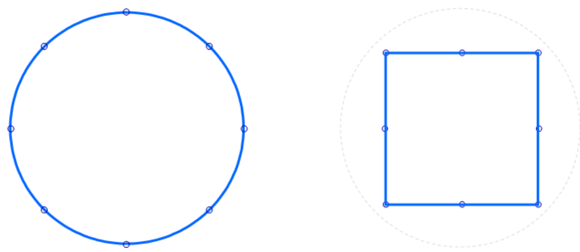

Figure B7. Collapse Mechanism with Eight Hinges

The equation derived from the equivalent beam method is also used to estimate the maximum peak in the observed force-crush characteristic by assuming *n* equal to 16:

$$\frac{\sigma_2}{\sigma_o} = 10.25\left(\frac{t}{D}\right)^2 \tag{B-15}$$

The corresponding estimates and test measurements are listed in Table B2, and compared in Figure B8.

In Section 3.2, nondimensional compressive strength is calculated by dividing the normalized peak stress by the relative density of the core. For the pipe core, the relative density is related to the core thickness and the pipe outer diameter by

$$\rho^* = \pi\frac{t}{D}\left(1-\frac{t}{D}\right) \tag{B-16}$$

from which

$$\frac{t}{D} = \frac{1}{2}\left[1-\sqrt{1-\frac{4}{\pi}\rho^*}\right]. \tag{B-17}$$

Combining equations (B-15) and (B-17) gives

$$\frac{\sigma_2}{\sigma_o\rho^*} = \frac{2.56}{\rho^*}\left[1-\sqrt{1-\frac{4}{\pi}\rho^*}\right]^2 \tag{B-18}$$

Results in Section 3.2 for the pipe cores are based on this equation.

Table B2. Plastic Collapse Estimates and Maximum Collapse Load Observed in Tests on Pipe Cores

D (inches)	σ_o (ksi)	A (in^2)	P_C (kip) Calculated (n = 16)	Test
2	52.3	144	302	273
3	43.0	144	110	128
5	37.1	150	36	37

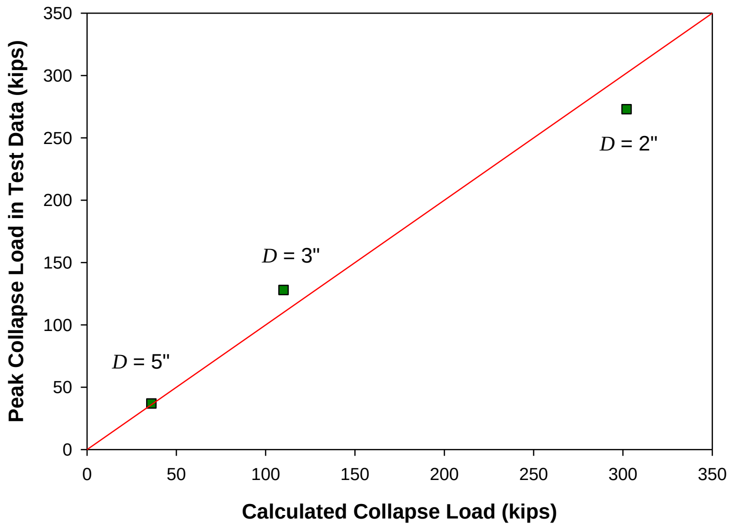

Figure B8. Comparison of Calculated and Measured Maximum Peak Loads

Similarly, from the videos and finite element simulations of the tests, the deformed pipe at the maximum plastic collapse load resembles a polygon that consists of 16 hinges, as shown in Figure B9. The figure shows that the sides of the polygon buckle inwards. In the videos and simulations, outward buckling occurs to the neighboring polygons or deformed pipes.

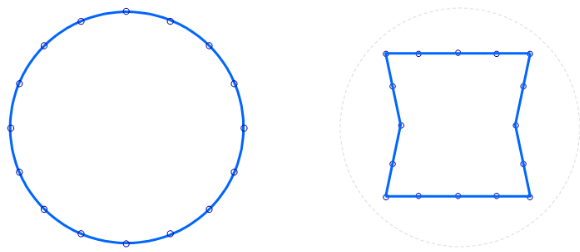

Figure B9. Collapse Mechanism with 16 Hinges

Figure B10 shows two video clips taken from the quasi-static compression test conducted on a sandwich panel with the 5-inch pipe core. The first clip shows the deformation of the cores at approximately 0.8-inch crush (or equivalently about 16 percent strain). In the second clip, the crush and the strain are about twice that of the first. Moreover, the idealized deformed shapes of the circular pipes are overlaid to show the resemblance to the collapse mechanisms assumed in the approximate limit analysis method.

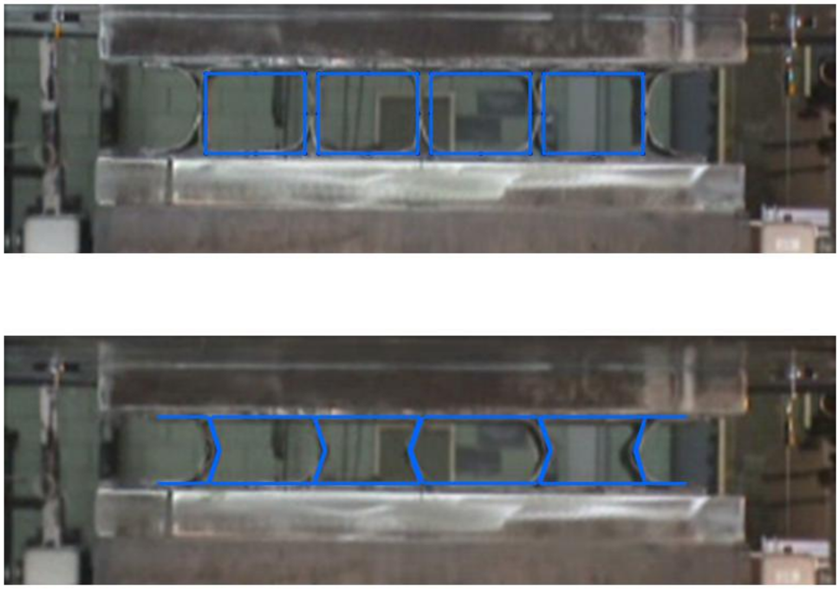

Figure B10. Annotated Video Clips from Compression Test on 5-Inch Pipe Core

B.2 Diamond Core Estimates

Similar limit analysis is applied to examine the collapse load for the idealized X-core without weld flats, shown in Figure B11, which is equivalent to the diamond core.

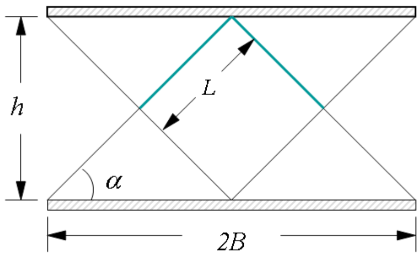

Figure B11. Sandwich Panel with Idealized X-Core

Under compressive loading, the upper half of the center diamond in Figure B11 is assumed to behave in a similar manner as a triangular truss with pinned supports subjected to an equivalent concentrated load (Figure B12):

$$P = \sigma_2 \cdot B \cdot b \tag{B-19}$$

where σ_2 is the compressive stress, B is the cell width, and b is the depth of the panel.

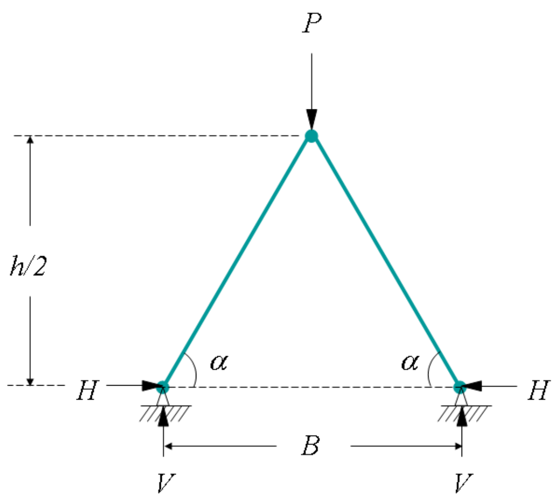

Figure B12. Triangular Truss with Pinned Supports

A free body diagram of the right-hand member of the triangular truss is shown in Figure B13, from which the compressive force in this member is equal to $P/2\sin\alpha$.

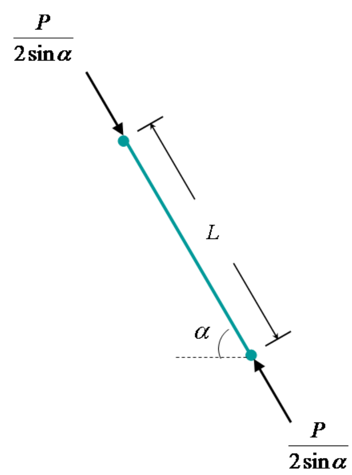

Figure B13. Free Body Diagram of Truss Member

Compressive yielding of this member occurs when the axial stress is equal to the yield strength

$$\sigma_o = \frac{P}{2tb\sin\alpha} = \frac{\sigma_2 B}{2t\sin\alpha} \tag{B-20}$$

where σ_o is the yield strength of the core material and t is the thickness of the core.

Therefore, the collapse strength of the idealized X-core or diamond core is given by

$$\frac{\sigma_2}{\sigma_o} = 2\left(\frac{t}{B}\right)\sin\alpha \qquad \text{(B-21)}$$

The relative density of the diamond core is estimated from

$$\rho^* = \frac{2}{\sin\alpha}\left(\frac{t}{B}\right) \qquad \text{(B-22)}$$

Assuming α equal to 45 degrees for the diamond core geometry and combining equations (B-21) and (B-22) gives

$$\frac{\sigma_2}{\sigma_o\rho^*} = 0.5 \qquad \text{(B-23)}$$

Results in Section 3.2 for the diamond core are based on equation (B-23).

The plastic collapse load associated with sandwich panels with the diamond cores used in the quasi-static compression tests are calculated from:

$$P_C = 2\sigma_o\left(\frac{t}{B}\right)\sin\alpha \cdot A \qquad \text{(B-24)}$$

where A is the loaded cross-sectional area of the panel.

Table B3 lists the characteristics of the test articles for the diamond cores. The table also lists the estimated plastic collapse load calculated from the limit analysis, which overestimates the collapse load observed in the two tests conducted on panels with the diamond core. The value of yield strength assumed in calculated collapse load is derived from the average of five tensile tests measurements on AISI 1010 steel of the same vintage used in the compression tests. Interestingly, if the nominal value of 44.2 ksi is assumed for the yield strength, the calculated collapse load is equal to 429 kilopounds (kip), which is in excellent agreement with the test results.

Table B3. Panel Characteristics and Collapse Loads for Tests on Diamond Cores

Characteristic	*Value*
Yield strength, σ_o	60.5 ksi
Area, A	144 in^2
Core height, h	2.62 in
Cell width, B	2.62 in
Angle, α	45^o
Calculated Collapse Load	588 kips
Measured Collapse Load (0047-13)	398 kips
Measured Collapse Load (0047-14)	420 kips

Appendix C. Force-Displacement Curves from Bend Tests and Analyses

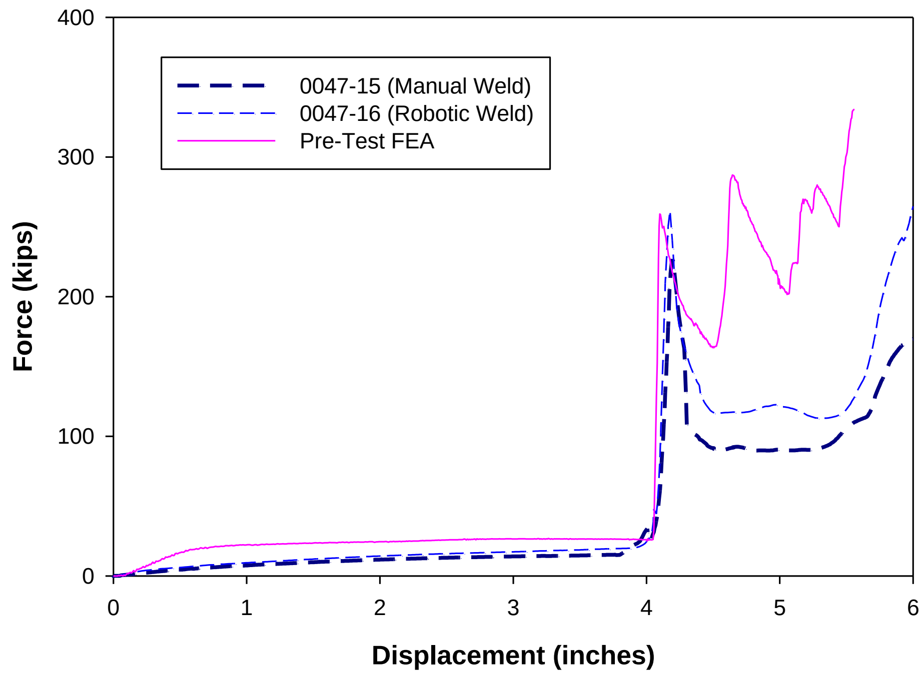

Figure C1. Diamond Cores Parallel to Supports with Solid Face Sheets

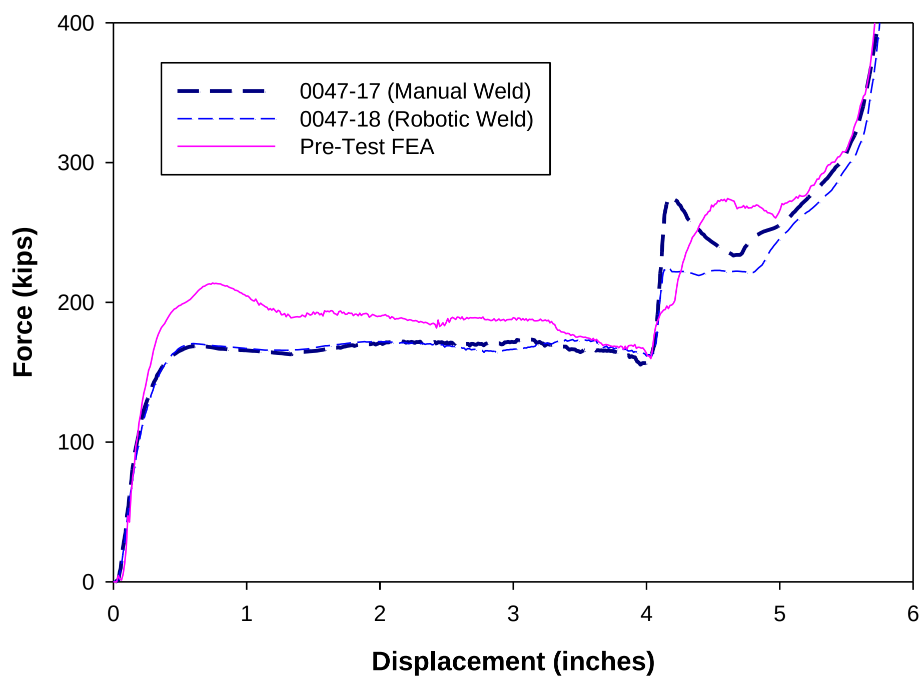

Figure C2. Diamond Cores Perpendicular to Supports with Solid Face Sheets

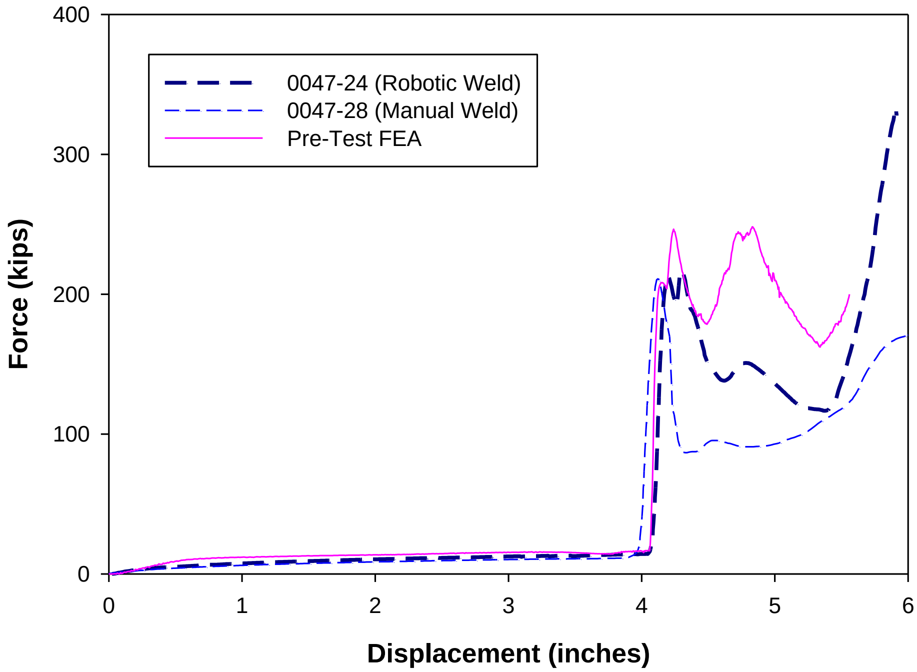

Figure C3. Diamond Cores Parallel to Supports with Strip Face Sheets

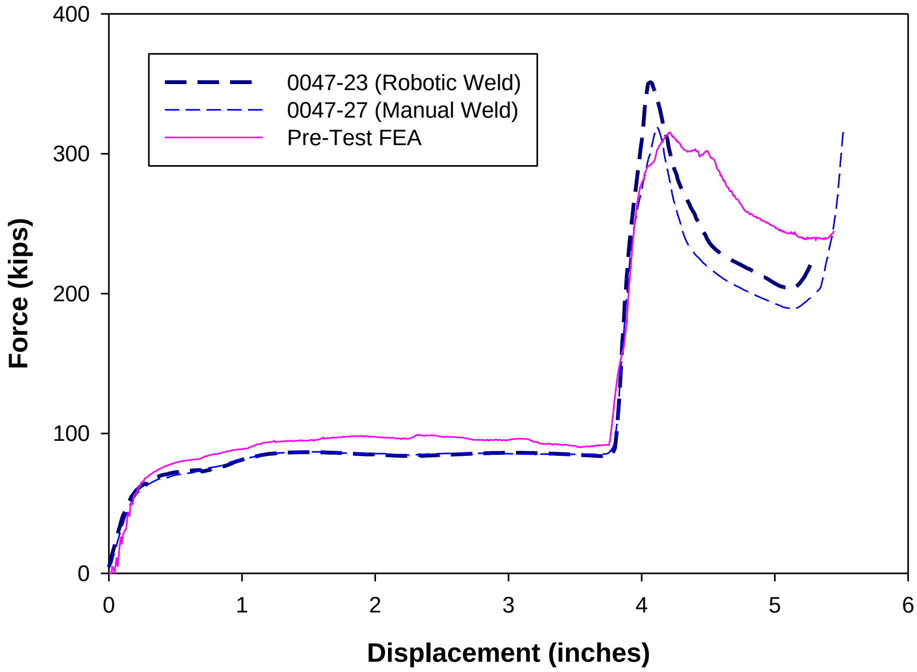

Figure C4. Diamond Cores Perpendicular to Supports with Strip Face Sheets

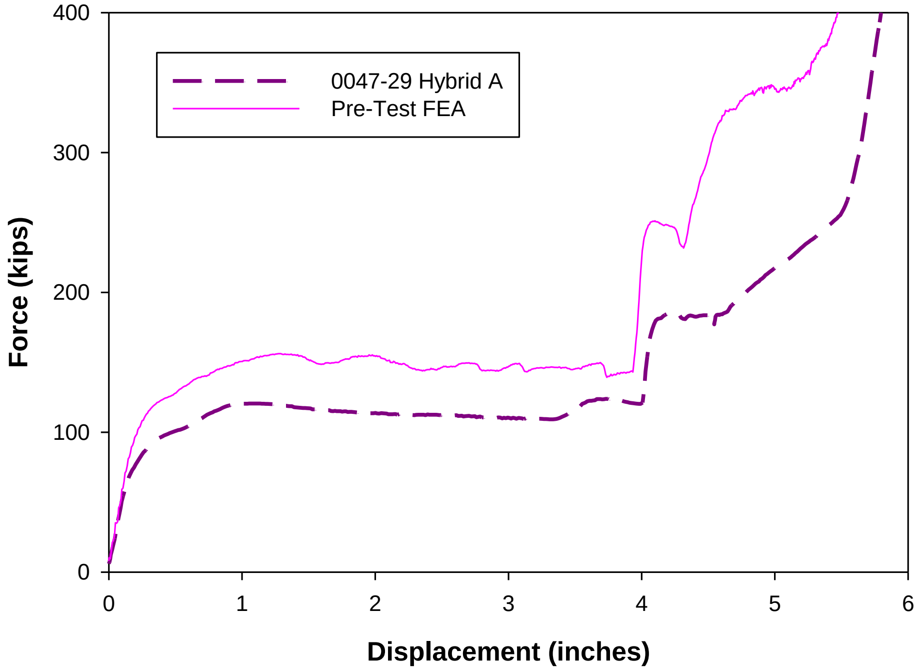

Figure C5. Diamond Cores Perpendicular to Supports with Hybrid A Face Sheets

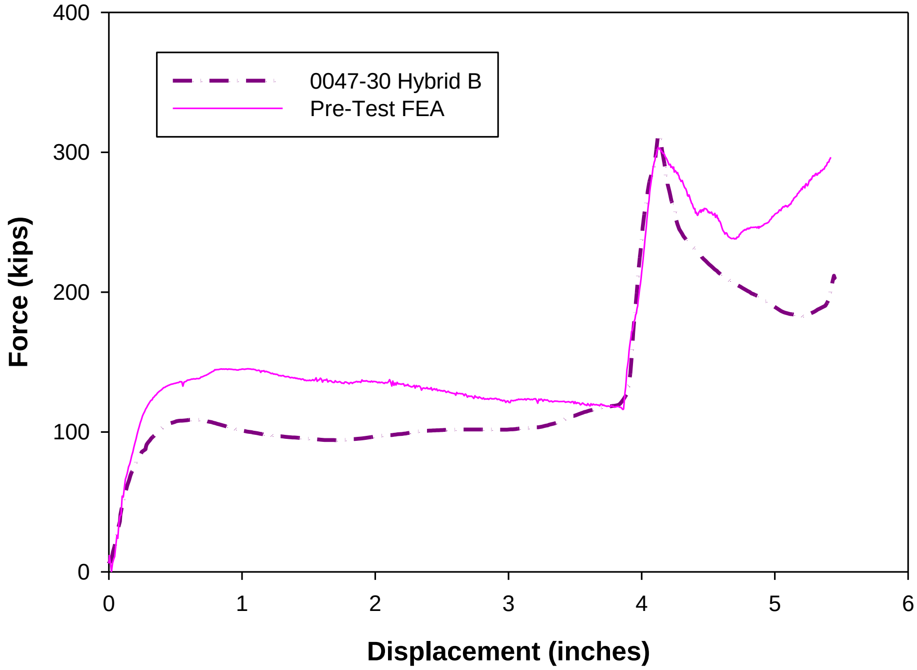

Figure C6. Diamond Cores Perpendicular to Supports with Hybrid B Face Sheets

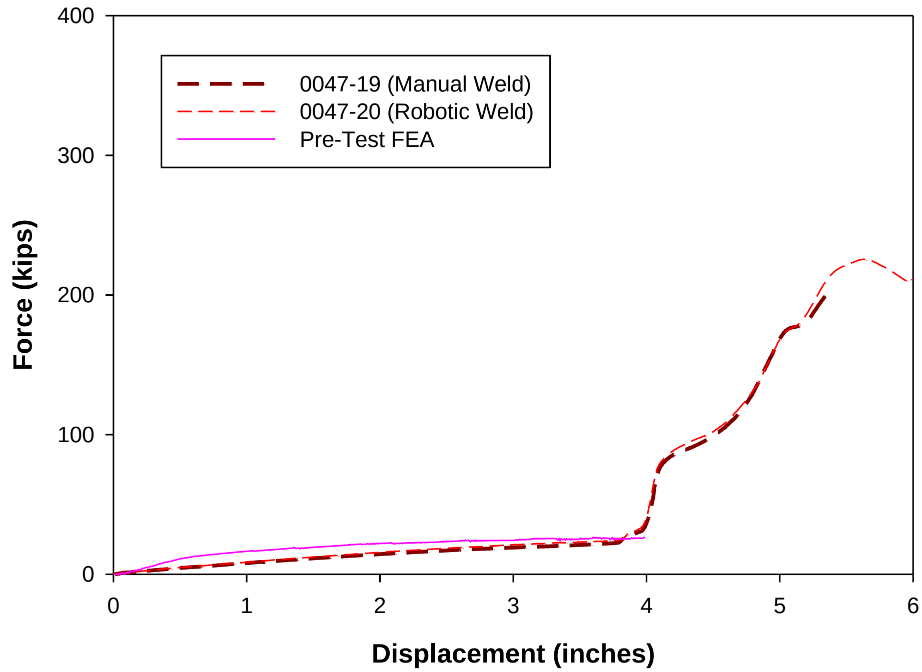

Figure C7. Pipe Cores Parallel to Supports with Solid Face Sheets

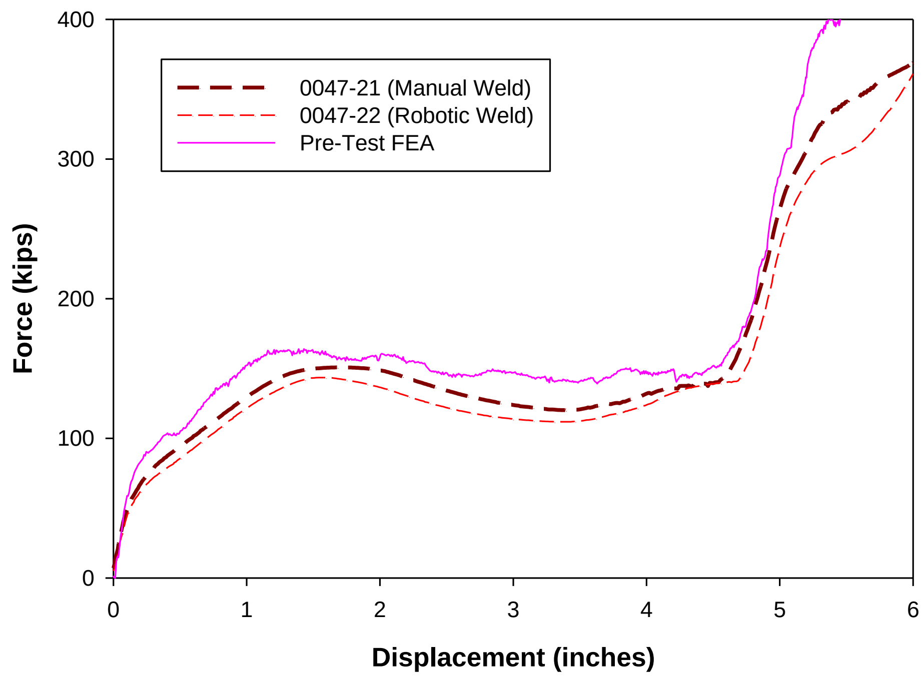

Figure C8. Pipe Cores Perpendicular to Supports with Solid Face Sheets

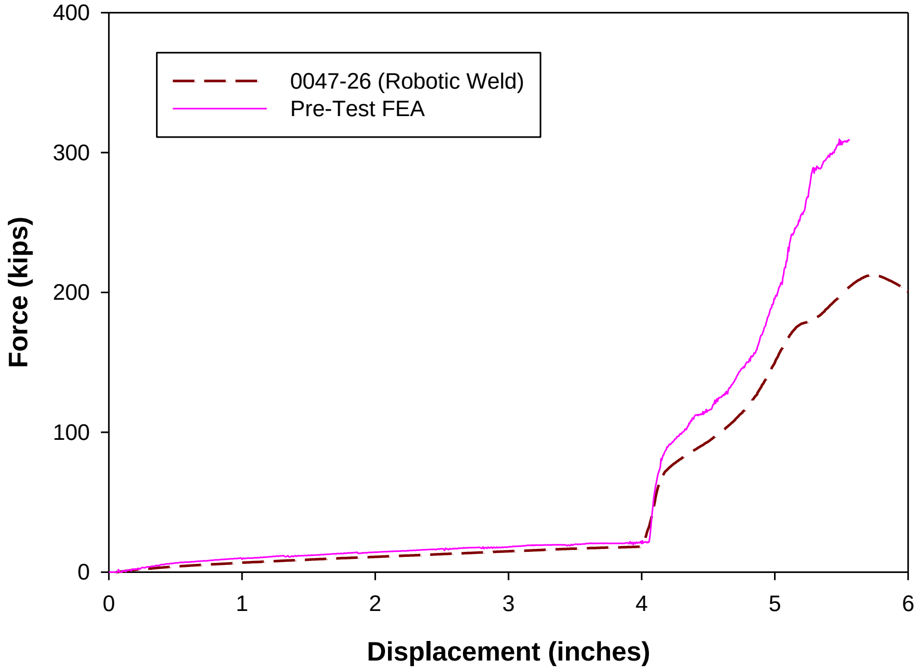

Figure C9. Pipe Cores Parallel to Supports with Strip Face Sheets

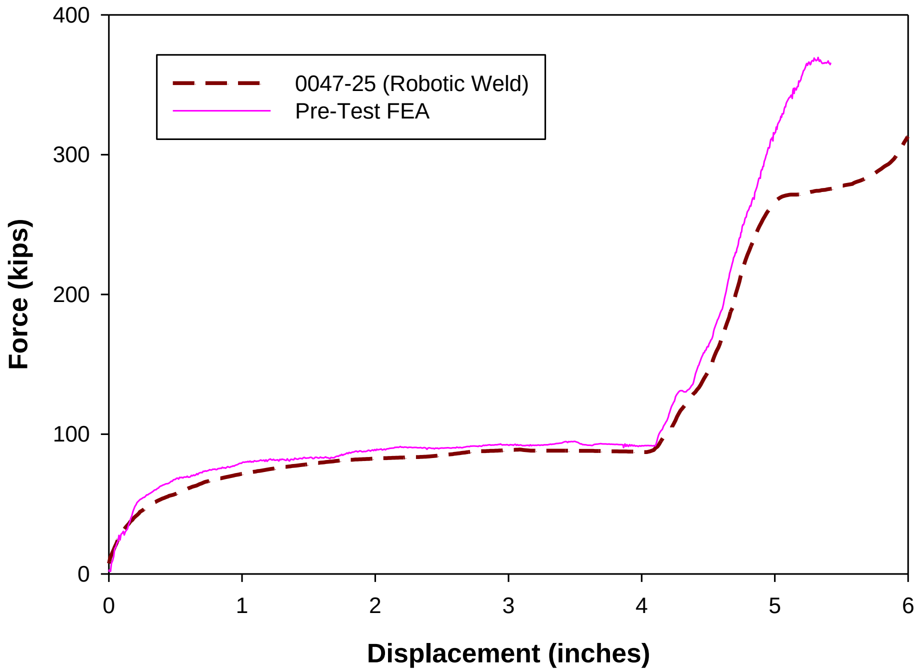

Figure C10. Pipe Cores Perpendicular to Supports with Strip Face Sheets

Abbreviations and Symbols

AAR	Association of American Railroads
AISI	American Iron and Steel Institute
ASTM	American Society for Testing and Materials
ATLSS	Advanced Technology for Large Structural Systems
CMI	Cellular Materials International, Inc.
FRA	Federal Railroad Administration
ft^2	square feet
in^2	square inch
kip	kilopound
ksi	kilopound per square inch
NTSB	National Transportation Safety Board
OTS	off-the-shelf
RAIRS	Railroad Accident/Incident Reporting System
RSI	Railway Supply Institute

A	area
D	pipe outer diameter
h_c	core height
ℓ, L	length
M_o	fully plastic moment
r	radius
t_c	core thickness
t_f	face sheet thickness
α	angle
ρ^*	relative density
σ_o	yield stress
σ_{peak}	peak stress